Bureau of Mines Report of Investigations/1985

Ground Control Study of a Mechanized Longwall Coal Operation in West Virginia

By Paul H. Lu

UNITED STATES DEPARTMENT OF THE INTERIOR

Report of Investigations 8929

Ground Control Study of a Mechanized Longwall Coal Operation in West Virginia

By Paul H. Lu

UNITED STATES DEPARTMENT OF THE INTERIOR
Donald Paul Hodel, Secretary

BUREAU OF MINES
Robert C. Horton, Director

Library of Congress Cataloging in Publication Data.

Lu, Paul H

Ground control study of mechanized longwall coal operation in West Virginia.

(Report of investigations / United States Department of the Interior, Bureau of Mines ; 8929)

Bibliography: p. 27.

Supt. of Docs. no.: I 28.23:8929.

1. Coal mines and mining—West Virginia—Safety measures. 2. Ground control (Mining). I. Title. II. Series: Report of investigations (United States. Bureau of Mines) ; 8929.

TN23.U43 [TN295] 622s [622'.8] 84-600266

CONTENTS

ILLUSTRATIONS

ILLUSTRATIONS--Continued

TABLES

UNIT OF MEASURE ABBREVIATIONS USED IN THIS REPORT

ft	foot	MPa	megapascal
in	inch	pct	percent
m	meter	psi	pound per square inch

GROUND CONTROL STUDY OF A MECHANIZED LONGWALL COAL OPERATION IN WEST VIRGINIA

By Paul H. Lu[1]

ABSTRACT

This Bureau of Mines report summarizes the analysis and evaluation of the field measurement results of a comprehensive ground control study conducted in a mechanized longwall coal mine in West Virginia. Emphasis is placed on the three basic ground control parameters: ground pressure, ground movement, and geomechanical properties. Specific topics include premining ground pressures, front-abutment pressure in the longwall panel, histories of pillar loading, differential roof-strata movement and bed separation, differential floor strata movement, entry roof-to-floor convergence, in situ moduli of rigidity of coal seam and roof and floor strata, and mechanical properties of coal and coal measures rocks.

[1]Mining engineer, Denver Research Center, Bureau of Mines, Denver, CO.

INTRODUCTION

Mechanized longwall mining in the United States is adopted from European practice and is relatively new. Because of geologic conditions such as shallower seams and strong roofs, and a different layout due to statutory requirements such as multiple entries, domestic longwall operations are conducted under different conditions. The stress distribution in the overlying strata above the seam and over the caved area, induced stresses over the pillars, are affected by the face length, panel layout, and overhanging immediate roof. The vertical pressure over the face supports, as evidenced by high chock capacity (up to 600 tons per unit), formation of pressure arch, etc., have not been clearly defined. Unique problems must be identified and solved by Bureau of Mines engineers and industry. The Bureau initiated a comprehensive ground control study at a mechanized longwall coal mine in West Virginia, with a contract to Harza Engineering Co., signed in May 1973 (1),[2] to develop simple and practical techniques for field measurement of ground control parameters. The contract study included measurements of ground pressures, strata movements, and geomechanical properties of coal measures rocks. The specific objective was to collect data with respect to longwall strata behavior that would make it possible to select the face and entry supports on a rational basis. The ultimate objective was to develop ground control design criteria, such as "integrity factors" for stability evaluation of longwall chain pillars (2), to improve the safety, reliability, and efficiency of the longwall mining in the United States.

This report summarizes the author's analysis and evaluation of the field data produced by the contractor and describes the in situ determined modulus of rigidity; other laboratory-determined mechanical properties are briefly described. Also presented are the methods and results of measurement of premining ground pressures, front-abutment pressures, histories of pillar loading in the longwall panels, differential roof-strata movements, differential floor lifts, and entry roof-to-floor convergence.

GEOLOGICAL AND OPERATIONAL SETTING

The longwall test site in the Federal No. 2 Mine of Eastern Associated Coal Corp. is located 25 miles west of Morgantown, WV. The mine was opened in 1968 and had only one operating longwall face during the study period. The face equipment consisted of a double-drum ranging-arm shearer and four-leg articulated chocks of 460-ton capacity with a designed yield pressure of 7,000 psi, and armored face conveyor. A section of the mine (fig. 1) that was typical of longwall operations shows the sequential progress of the two longwall panels instrumented and tested under the project. The two instrumented panels were 2,530 ft long; panel 1 was 430 ft wide and panel 2 was 410 ft wide. The two panels were separated by a 210-ft-wide, three-entry-gate system consisting of a 17-ft-wide belt entry, a 14-ft-wide air entry, and a 14-ft-wide middle supply entry (fig. 1). Coal was mined from the Pittsburgh seam, one of the largest and most valuable coal seams in the United States. The extraction height was 76 in, with approximately 18 in each of coal being left on the roof and on the floor to improve stability and to control horizon. The coal seam is moderately friable and is separated into splits by thin continuous beds of pyritiferous shale.

The entry roof was supported by 7-ft-long roof bolts and wooden planks. The tailgate-entry supports were supplemented by two rows of wooden cribs. Each panel was mined by retreating from west to east during an approximate 10-month period. (Face positions at different time

[2]Underlined numbers in parentheses refer to items in the list of references preceding the appendixes.

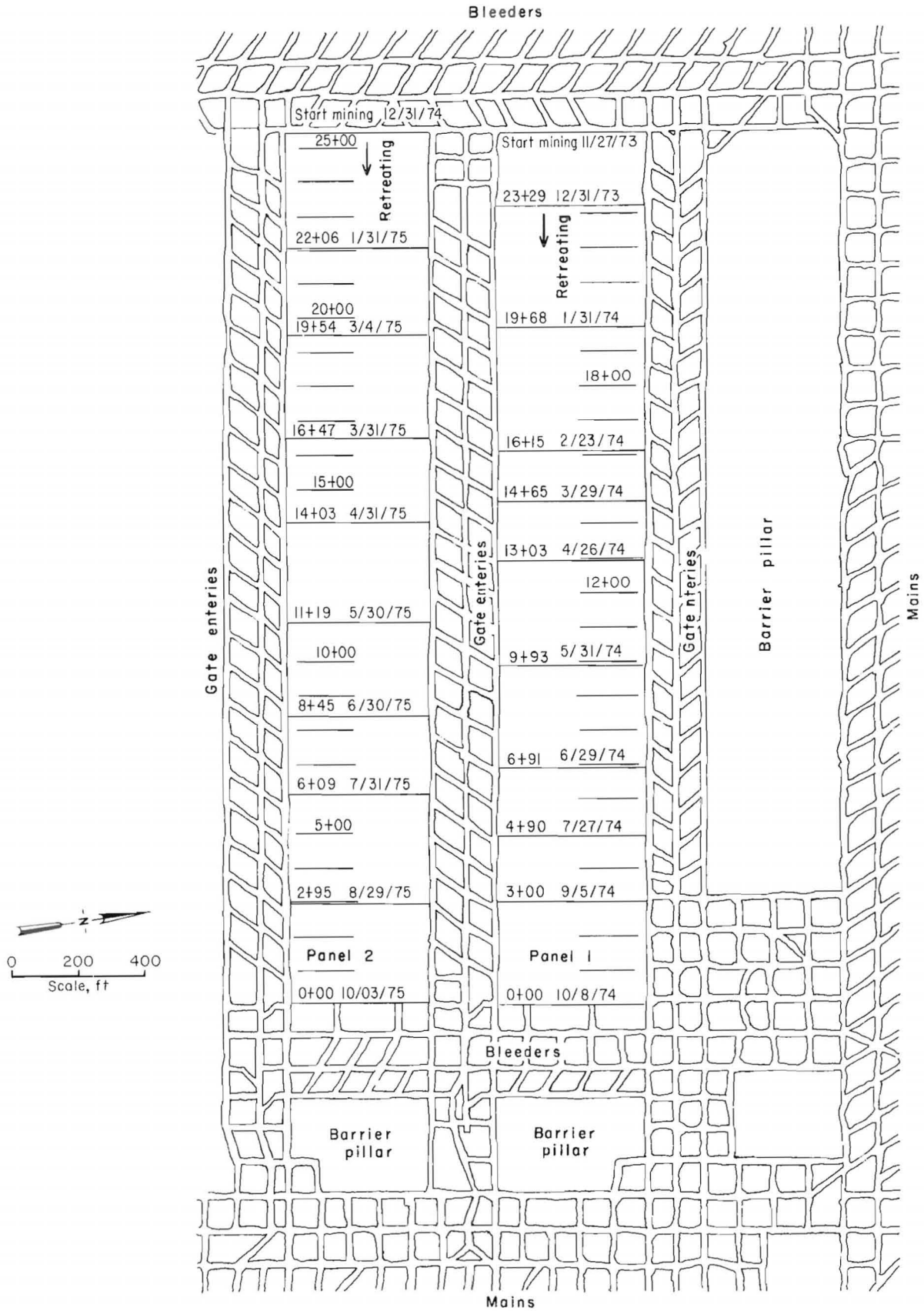

FIGURE 1. - Mining plan and progress schedule.

intervals are shown in figure 1. For example, "23 + 29" on 12/31/73 means the longwall face was located 2,329 feet away from the finishing line 0+00 of the retreating panel 1.)

The overburden, from approximately 750 to 1,000 ft thick, consisted of shale, sandstone, and limestone. Immediate roof strata consisted of shale and shaly limestone, but floor rocks were predominantly shale. The structural geology of the area was characterized by nearly flat-lying to gently dipping beds and gentle folds. The beds dip to north or south less than 10°. No major faults are known to exist. Two prominent sets of joints intersect at approximately 60° to 80° to each other. The bearing of the face cleats (major joints) ranges from N 55° W to N 90° W and dips from S 83° to N 89°. The bearing of the butt cleats (minor joints) ranges from N 5° E to N 45° E, and dips from N 78° to S 80°. The gate entries and crosscuts in the mine were driven approximately parallel to these cleats.

GEOMECHANICAL PROPERTIES

Mechanical properties such as strengths and deformation moduli are among the most important parameters for ground control and mine design. An extensive program of laboratory testing of coal and rock samples was performed by the Rock Mechanics and Explosives Research Center of the University of Missouri-Rolla under a subcontract with Harza Engineering (1). Comprehensive in situ modulus of rigidity tests were also conducted by Harza Engineering Co. (1) and the Bureau of Mines separately.

The correlation between laboratory tested property and in situ determined property, however, is not discussed here.

MECHANICAL PROPERTIES

Uniaxial and triaxial compressive strengths, tensile strength, Young's modulus, Poisson's ratio, and modulus of rupture of coal and roof and floor rocks were determined from NX-size (2.155 in) diamond drill cores of the roof and floor strata and the coal seam. The results of these tests on selected roof and floor core specimens are shown in figures 2 and 3 with the strata correlation; however, the property values shown are those normal to bedding plane only. The property values for shale are comparatively high due to lower recovery of shale core. The summary of mechanical properties of the coal is listed in table 1.

IN SITU MODULUS OF RIGIDITY

The Bureau of Mines determined moduli of rigidity of coal seam and roof rocks using cylindrical hydraulic borehole pressure cell (CPC) dilation tests (3). All CPC's installed for existing ground pressure measurements were also used for these tests. In addition, 20 measurements were made in the coal seam in 4 horizontal 18-ft holes. Two vertical holes, approximately 40 ft and 25 ft in the roof and in the floor were used to obtain the modulus-of-rigidity profiles of immediate roof and floor strata. The results of 39 tests indicate that the modulus of rigidity of the Pittsburgh coal seam is $(0.307 \pm 0.015) \times 10^6$ psi at the 95-pct confidence level. The modulus of rigidity of the 15-ft-thick limestone bed located 12 ft above the Pittsburgh seam is $(2.126 \pm 0.991) \times 10^6$ psi from four selected tests at the 95-pct confidence level. The modulus-of-rigidity profile of the coal measures was also determined by means of geophysical logging conducted by Birdwell Division of Seismic Service, Inc., under a subcontract with Harza Engineering, at 1-ft intervals from the surface to approximately 200 ft below the Pittsburgh seam. The results of borehole dilation tests and geophysical logging are shown in figures 4 and 5 for comparison. The modulus values obtained from the CPC tests generally will agree with those obtained from geophysical logging for coal and shale.

TABLE 1. · Summary of mechanical properties of coal seam

	Uniaxial compressive strength (L/D = 2), psi	Young's modulus 10^6 psi	Poisson's ratio[1]	Tensile strength,[2] psi	Modulus of rupture, psi	Specific gravity
Coal.....	2,621	0.62	0.354	158 (68)	224	1.29
Standard deviation.....	533	0.14	0.072	62 (37)	122	0.046
Number of tests.	12	11	4	6 (13)	3	6

[1]Excluding those >0.48.

[2]Tensile strength perpendicular to bedding plane; numbers in parentheses show tensile strength parallel to bedding plane.

The triaxial compressive strength of coal is as follows, in pounds per square inch:

Confinement	Strength
0.....	2,620
500.....	4,090
1,000.....	6,350
1,500.....	8,115
2,000.....	10,925

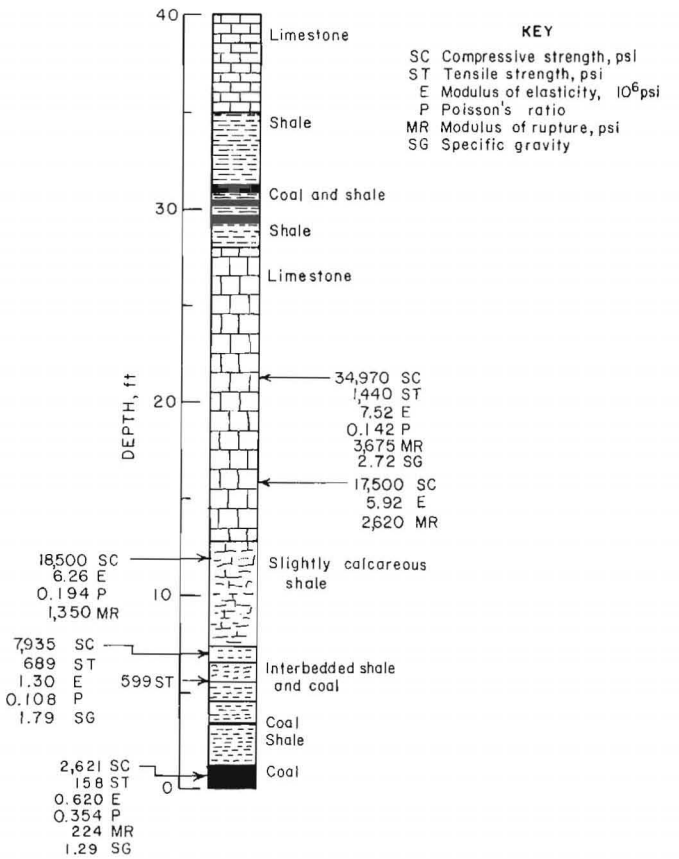

FIGURE 2. - Mechanical properties of selected roof core samples.

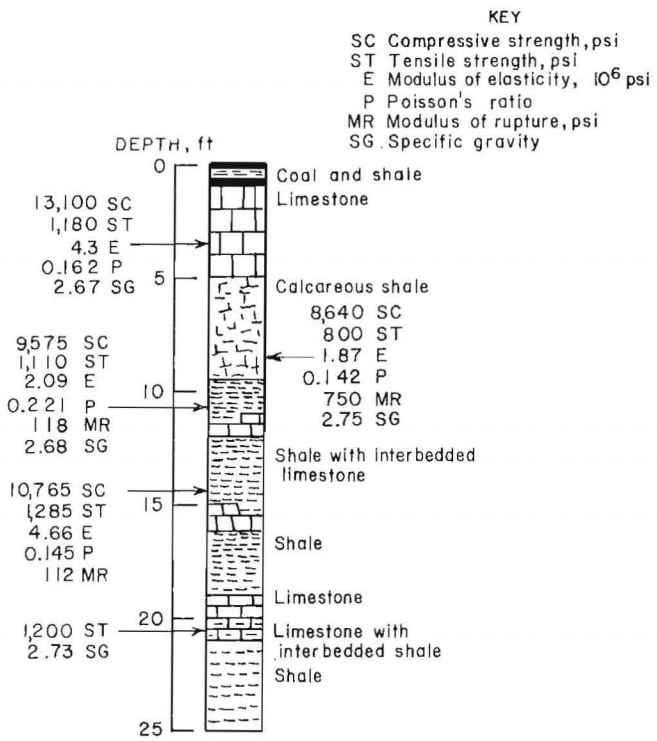

FIGURE 3. - Mechanical properties of selected floor core samples.

GROUND PRESSURES

The ground-pressure-monitoring instrumentation was intended to cover the premining ground pressures, front-abutment pressures in the longwall panels, and loading histories of gate-entry and bleeder-entry pillars, and barrier pillars, as shown in figure 6. The instrumentation array was determined in accordance with the surface subsidence surveying monumemt array, which is not included in this report.

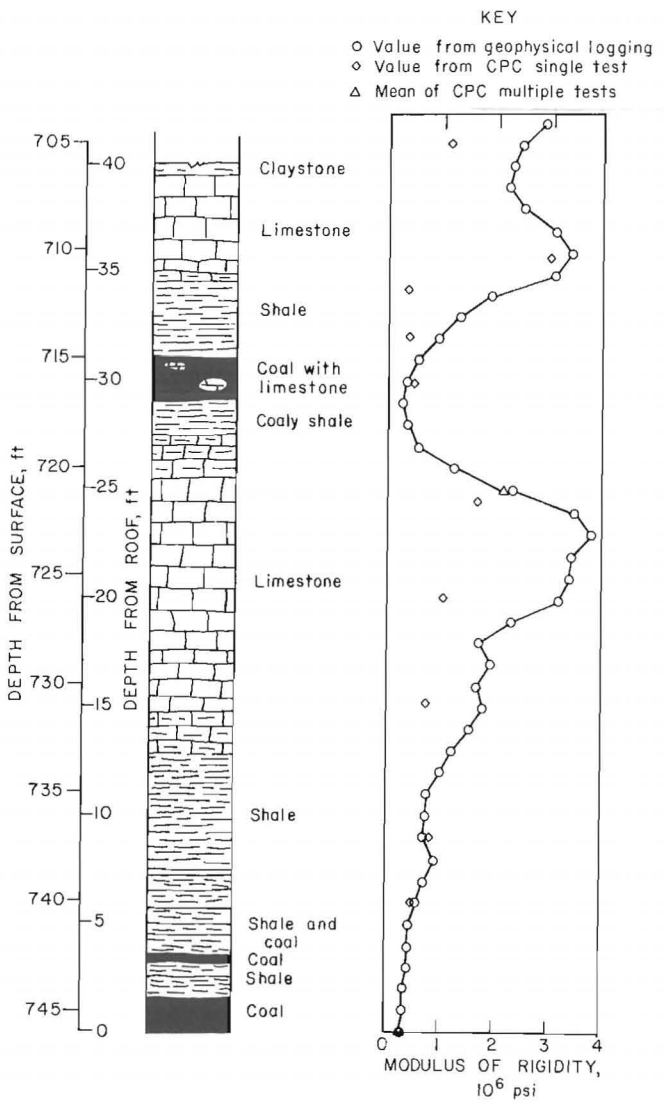

FIGURE 4. - Modulus-of-rigidity profile of roof strata.

GROUND PRESSURE PRIOR TO LONGWALL OPERATION

By assuming coal is a viscoelastic material, the ground pressures existing in the two-panel area, at the horizon of the Pittsburgh seam, prior to longwall operation, were determined by pressure convergence tests (4) using a combination of one CPC and two preencapsulated flat hydraulic borehole pressure cells (BPC) installed in a single hole drilled into the undisturbed area (fig. 7). The BPC's determine the ratio of ground stresses in two perpendicular directions and the CPC determines their sum. The biaxial ground stresses were consequently determined by the equilibrium pressures of the three cells, obtained from the respective cell pressure convergence curves, as shown in figure 8. The theoretical considerations for determination of ground pressure existing in a viscoelastic rock mass

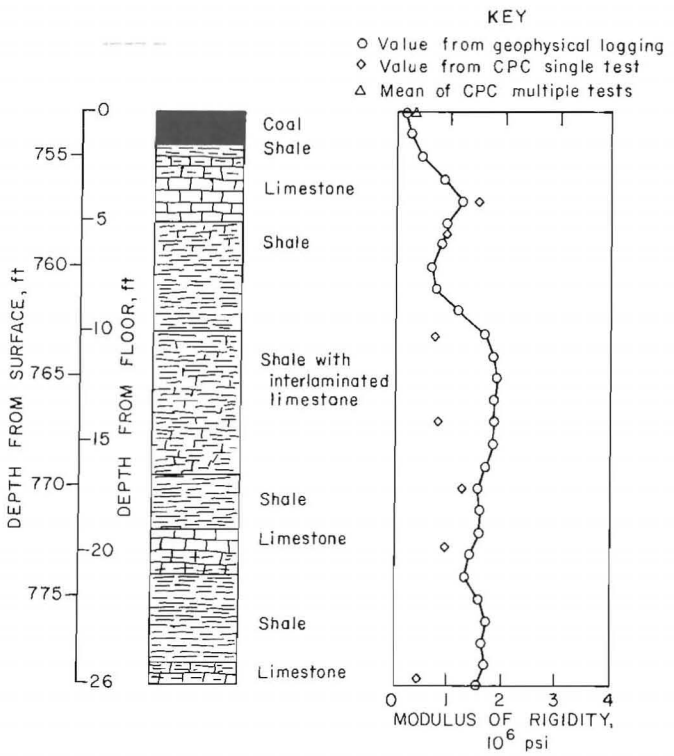

FIGURE 5. - Modulus-of-rigidity profile of floor strata.

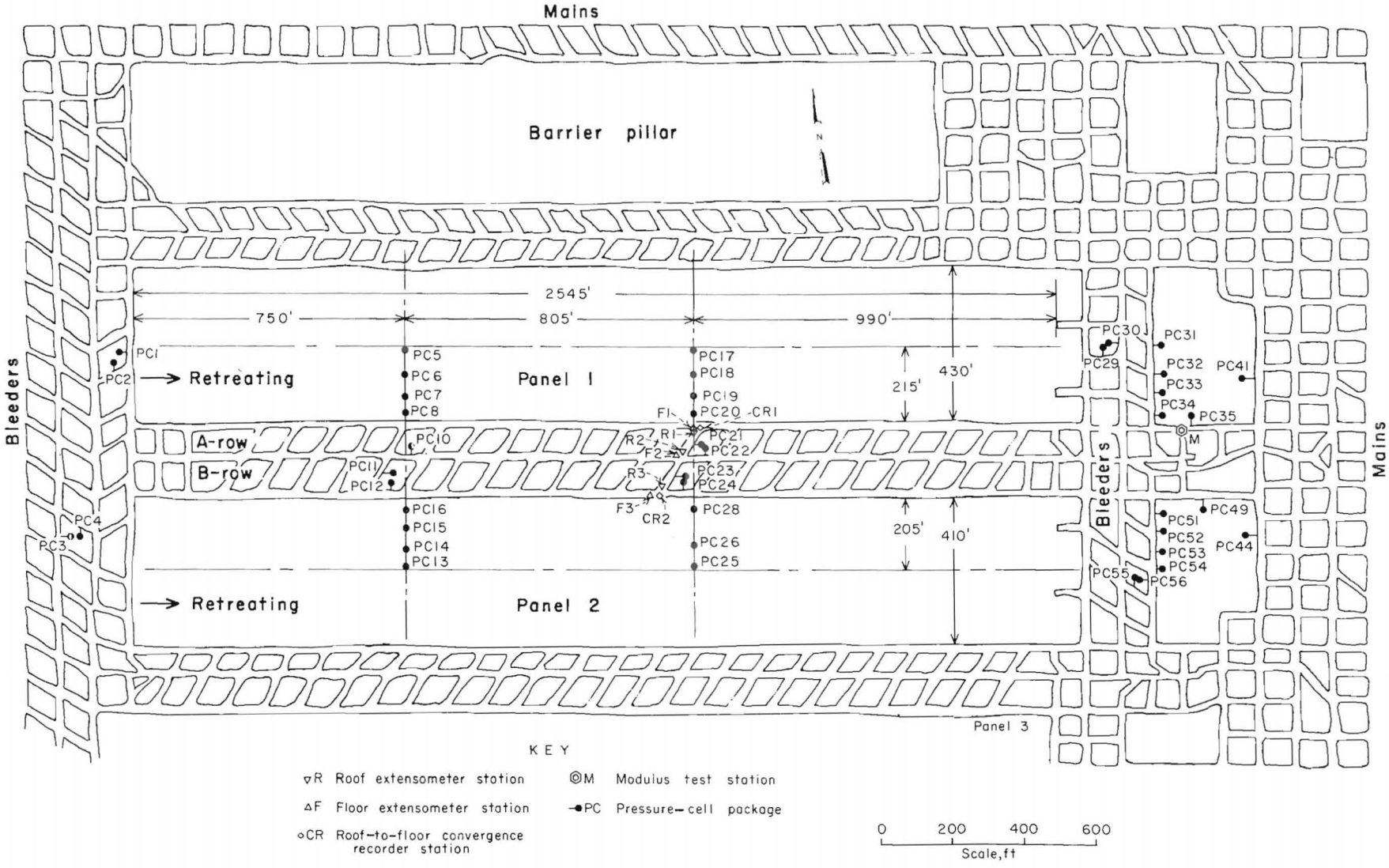

FIGURE 6. - Instrumentation plan.

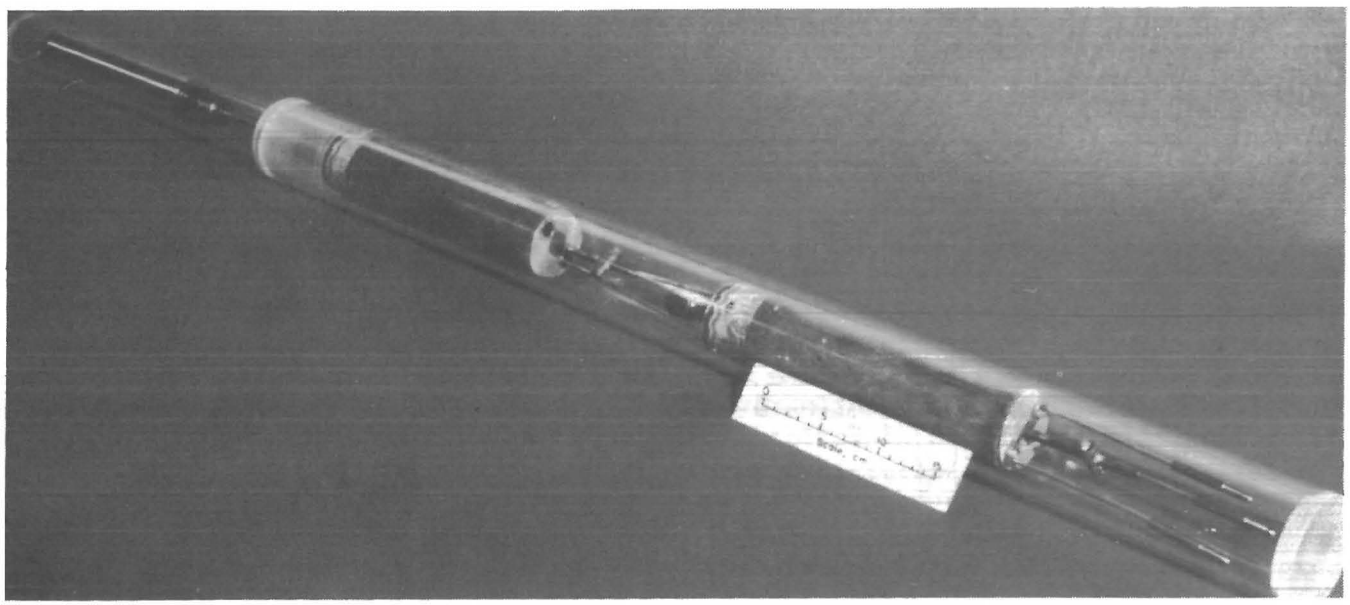

FIGURE 7. - Pressure-cell package consisting of one CPC and two BPC's.

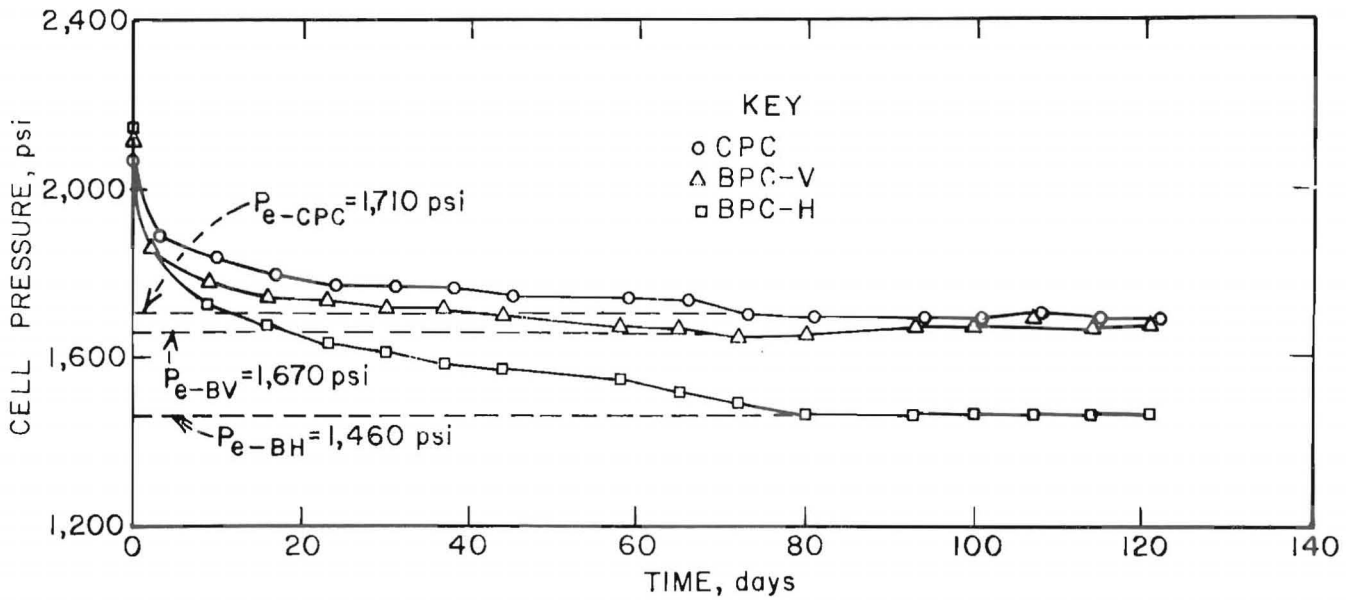

FIGURE 8. - Cell-pressure-convergence curves and cell-equilibrium pressures for PC49.

by use of borehole pressure cells are abstracted from reference 4 and included in appendix A.

The vertical pressure (N_V) and horizontal pressure (N_H) existing in the seam at site PC49 (fig. 6) can be calculated from the cell equilibruim pressures P_{e-CPC} = 1,710 psi, P_{e-BV} = 1,670 psi, and P_{e-BH} = 1,460 psi (fig. 8) by employing appendix equations A-9 and A-14. In these two equations, ν(0.345) is Poisson's ratio determined by the laboratory tests (table 1 and figure 2), $Q = P_{e-BH}/P_{e-BV}$, and S is transverse sensitivity of a BPC, which is 0.185 as calculated from the geometry of the cell. From these two equations, $N_V + N_H$ = 2,647 psi, N_H/N_V = 0.83, N_V = 1,447 psi and N_H = 1,200 psi are obtained. Their rounded-off numbers, N_V = 1,450 psi and N_H = 1,200 psi, are listed in table 2 and plotted in figure 9.

TABLE 2. -- Results of premining ground-pressure measurements

Location[1]	Depth of measurement hole, ft	Vertical pressure (N_V), psi	Horizontal pressure (N_H), psi[2]		$\frac{N_H}{N_V}$	BPC response ratio (K)[3]
			N_H (N-S)	N_H (E-W)		
PC1	24	1,270	1,210		0.95	1.14
PC2	23	1,550		1,080	.70	.80
PC3	22	1,500	1,290		.86	1.05
PC4	23	1,250		1,570	1.25	.97
PC5	208	840		1,360	1.62	ND
PC6	138	990		1,120	1.13	ND
PC7	78	1,360		1,270	.93	1.09
PC8	29	1,280		880	.69	1.11
PC10	23	1,020		1,390	1.36	.82
PC11	23	1,250	1,250		1.00	ND
PC12	24	1,230		1,480	1.20	.77
PC13	189	1,300		1,240	.95	1.14
PC14	129	1,590		1,270	.80	.86
PC15	80	1,680		1,340	.80	.76
PC16	27	1,160		1,400	1.21	ND
PC17	208	1,090		910	.83	ND
PC18	135	1,000		1,000	1.00	ND
PC19	79	1,150		1,020	.89	ND
PC20	29	870		990	1.14	1.09
PC21	23	900	690		.77	ND
PC22	24	1,000		1,100	1.10	ND
PC23	23	1,090	770		.71	ND
PC24	24	1,060		1,190	1.12	.81
PC25	189	980		1,340	1.37	1.18
PC26	127	1,260		1,060	.84	ND
PC28	28	1,170		1,150	.98	ND
PC29	22	850		1,160	1.36	1.17
PC30	24	840	1,100		1.31	1.19
PC31	9	1,320	1,230		.93	1.03
PC35	24	1,320		1,080	.82	1.10
PC41	24	1,240	1,040		.84	1.10
PC44	24	1,130	1,270		1.12	.88
PC49	24	1,450		1,200	.83	1.00
PC52	9	1,380	1,290		.93	.94
PC55	23	1,180		1,050	.89	1.18
PC56	23	1,500	1,330		.89	.84

ND Not determined.

[1]Missing PC numbers indicate either instrumentation failure or that instrumentation was not used for this measurement.

[2]Horizontal pressure measurement was taken in only 1 direction (north-south or east-west) at each location.

[3]$K = \frac{\text{BPC equilibrium pressure}}{\text{Effective directional ground pressure}}$. Average K = 1.00±0.05.

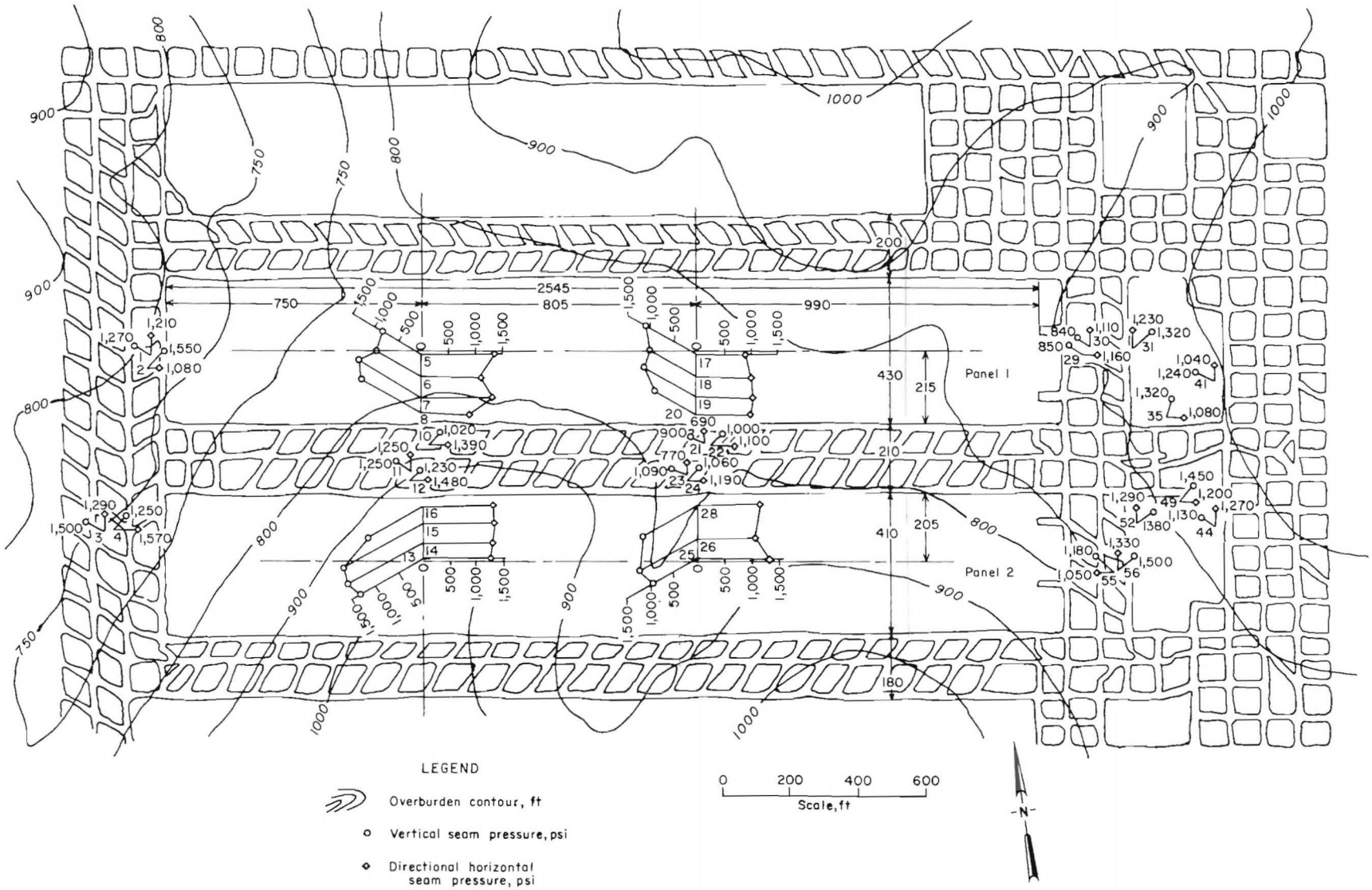

FIGURE 9. - Ground-pressure distribution map.

With this technique, the vertical ground stress prior to longwall operation, ranging from 840 to 1,680 psi, was determined as shown in table 2 and figure 9. The variation of the vertical stress was dependent on the thickness of overburden and coal extraction ratio at the measuring location. The horizontal ground stress was in the range of 690 to 1,570 psi. These results reveal that the vertical pressures agree with the theoretical values derived from the overburden weight. The horizontal pressure ranges from 69 to 162 pct of the vertical pressure. Theoretically, the ratio of the horizontal stress to vertical stress should be 55 pct for $\nu = 0.354$, by assuming the coal is nearly elastic; therefore, the tectonic stress in this area is very significant in both north-south (N-S) and east-west (E-W) directions. The vertical pressure profiles across the panels show wavy shapes, with their peaks at approximately 20 pct of the panel width inside the ribs (fig. 9). This phenomenon suggests a formation of pressure arch over the 210-ft-wide gate-entry system with its abutments located at 20 pct of the panel width inside the ribs.

The in situ BPC response ratio K, which is the ratio of BPC equilibrium pressure to the effective directional ground pressure, is 1.00 at the 95-pct confidence level with standard deviation of 5 pct, as shown in table 2. For example, K(PC49) was derived as follows: $K_{(PC49)} = P_{e-BV} / (N_V + S \times N_H) = 0.998$ or $K_{(PC49)} = P_{e-BH} / (N_H + S \times N_V) = 0.995$. With this response ratio, the absolute values of biaxial ground stresses and stress changes can be determined with a combination of two BPC's installed in a single drill hole (5). The basic concepts of mining-induced stress measurement with hydraulic borehole pressure cells are abstracted from reference 5 and included in appendix B.

FRONT-ABUTMENT PRESSURE IN LONGWALL PANEL

From periodic pressure gauge readings before and during face passage and continuous-pressure-recorder charts for BPC's installed in the longwall panels, the vertical front-abutment pressure profiles are drawn (figs. 10-11). Noticeable increase of mining-induced seam pressure began when the face distance was approximately 160 ft in panel 1 and 170 ft in panel 2, approximately 0.18 to 0.2 times the overburden thickness. The abutment pressure rose gradually until the face was 50 ft away; thereafter, the rate of increase accelerated until the abutment pressure reached the peak value at approximately 6.9 ft distance, which is approximately equal to the extraction height. The pressure rapidly dropped to zero or below the premining seam pressure at the actual face through the 6.9-ft-wide yielded zone. These measured results reveal that the width of the abutment zone is approximately 160 to 170 ft (0.18 to 0.20 times the overburden thickness) including the 6.9-ft (extraction height) wide yielded zone.

The idealized profiles of the vertical front-abutment-pressure increment across the panel, which were composed of data from the two panels, are plotted in figure 12. The profiles are not symmetrical about the central axis of the panel because the panel adjacent to the tail entry of panel 2 had been mined out and the roof had caved. The skewness is amplified when the longwall face has approached the pressure cells. The central one-third of the panel undergoes the lowest abutment pressure; the tail entry (gob side) abutment is 2 to 3 times greater than that of the head entry side. This is evidently due to the interaction of side-abutment pressure of the inter-panel entries. The side-abutment pressure is higher on the tail entry side because its adjacent panel has been extracted and the overburden pressure has been transferred onto the active panel.

The width of the front abutment and the magnitude of the vertical pressure in figures 10 and 11 can be used as criteria for entry support design because the loads applied to support the entry roof should be proportional to the seam pressure. Therefore, for that portion of entry where the front-pressure abutment

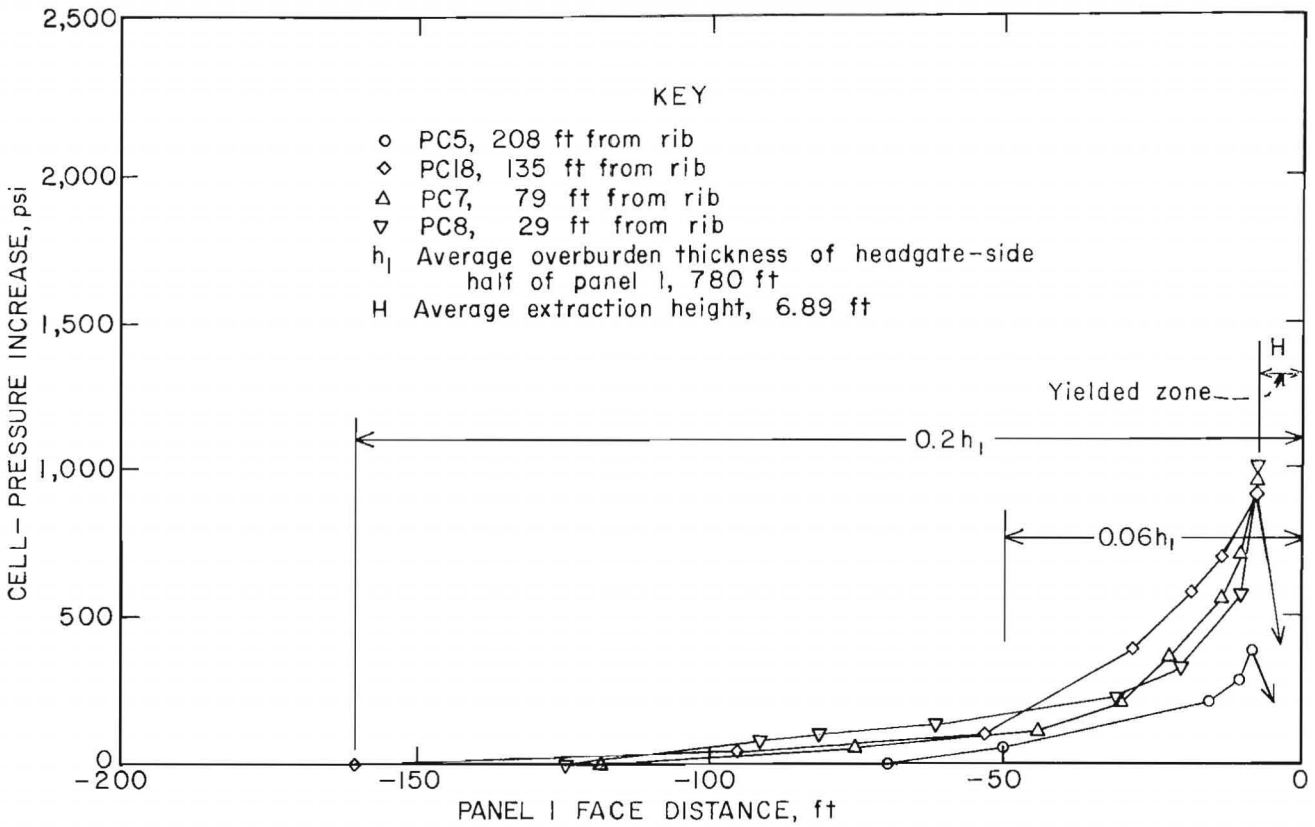

FIGURE 10. - Profile of vertical front-abutment pressure of headgate-side half of panel 1 during extraction of panel 1.

forms, the support density should be increased in proportion to the increase in the abutment pressure. Such reinforcement can be achieved by adding cribs or hydraulic props.

HISTORIES OF PILLAR LOADING

Histories of pillar loading in terms of mining-induced pressure changes were observed with BPC's installed in the active mining areas. Three types of pillars were investigated: gate-entry pillar, bleeder-entry pillar, and barrier pillar between the bleeder entry and the mains. Throughout this report, the "face distances" refer to the plane distances between the monitoring instrumentation and the longwall face. Negative distance indicates that the instrumentation plane is in the solid area and positive distance indicates that the instrumentation plane is in the gob area.

Gate-Entry Pillars

The loading histories of the gate-entry pillars shown in figure 13 are depicted by a plot of the cell pressure changes that were recorded before, during, and after face passage. Pressure in the center portion of the pillar was measured by pressure cells installed 22 to 24 ft inside the 82- by 100-ft pillars. The vertical loading induced by the extraction of panel 1 on both A-row and B-row pillars (see figure 6) initially increased at approximately -300 ft. The loading continued to increase until the face had reached the cells. The loading still continued to increase, but at a reduced rate until this face had retreated approximately 600 ft beyond the cells; thereafter, the loading gradually stabilized (figures 13*A* and 13*D*).

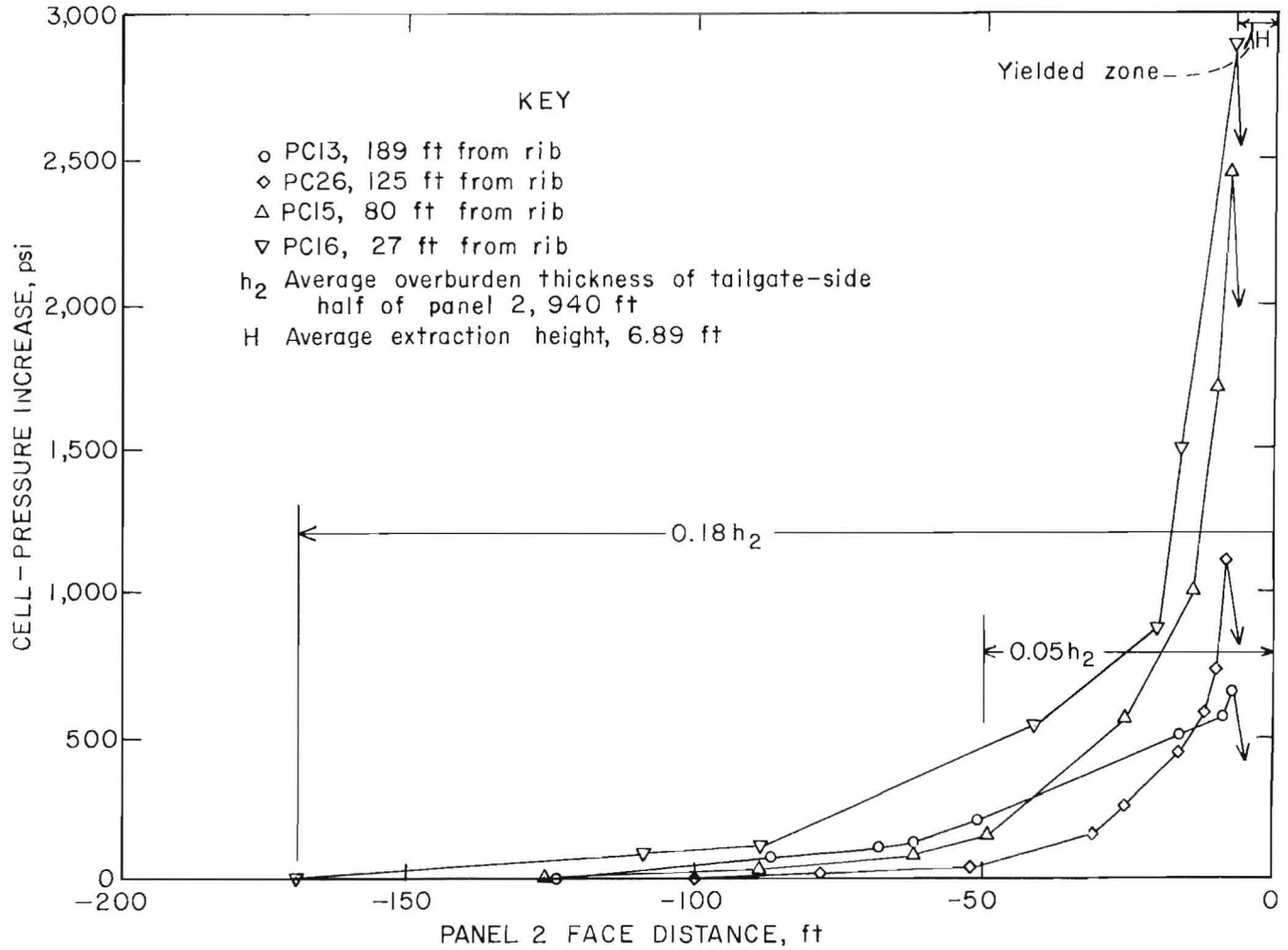

FIGURE 11. - Profile of vertical front-abutment pressure of tailgate-side half of panel 2 during extraction of panel 2.

The vertical loading induced by the extraction of panel 2 on the A-row pillar started to increase at -400-ft face distance up to -250-ft face distance, where the pillar apparently had a local failure. However, the residual strength continued to support the much-reduced load until the face had reached -150-ft distance (data collection was terminated at this time due to excessive roof falls and pillar rib spalling), as shown in figure 13*A*.

The vertical loading induced by the extraction of panel 2 on B-row pillars started to increase at -300-ft face distance. It peaked at zero face distance with a 300-pct increase (fig. 13*D*). Shortly thereafter, the pillar collapsed. This event suggests that the overburden weight originally distributed over panel 1 was transferred onto panel 2 rather than onto the interpanel pillars after panel 1 had been extracted. This effect is due to the pressure arch over the gate-entry system, which formed shortly after the entries had been developed. Then the increased overburden load over panel 2 was transferred back onto the interpanel pillars, especially onto the B-row pillars, when panel 2 was extracted.

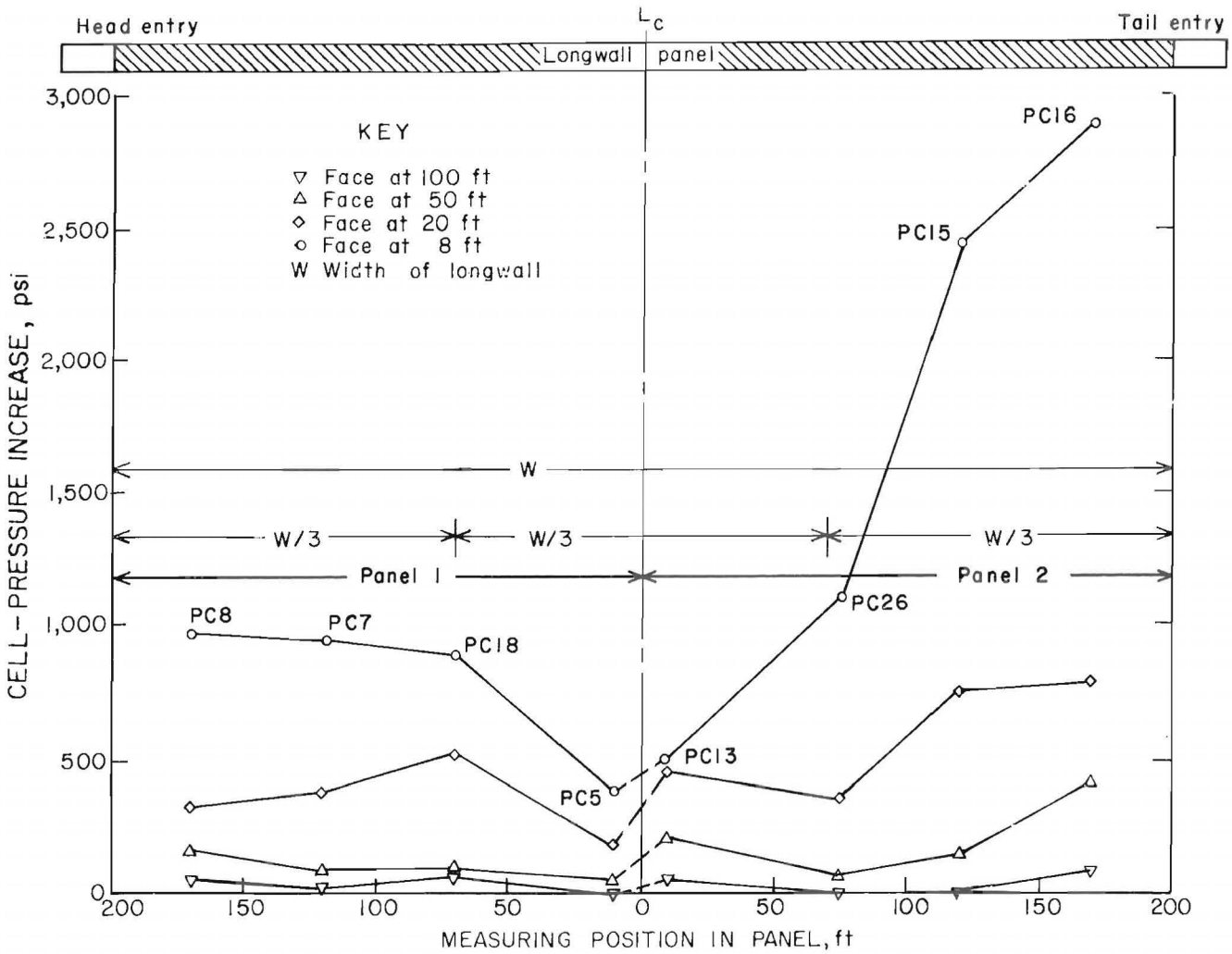

FIGURE 12. - Idealized schematic of progressive profiles of vertical-pressure increase across panel.

The horizontal loading in both directions, parallel and perpendicular to mining direction, generally decreased gradually following the face advance. However, when the longwall face had approached within 100 ft, it increased moderately up to zero face distance (fig. 13, *B-C*, *E-F*).

A comprehensive study of gate-entry pillar-loading history may lead to new approaches of longwall pillar design such as the "integrity factor approach" (2). The vertical-pressure profile across the pillar gives the total pillar load. The horizontal-pressure profile yields a strength profile, which in turn gives the total pillar strength. Thus the "integrity factor," defined as "the ratio of total strength to total load under the respective profiles," can be derived.

Bleeder-Entry Pillars

Starting-End Pillars

The loading histories of the starting-end bleeder-entry pillars are generally those of unloading in accordance with the face advance, as shown in figure 14. The vertical pressure in the first-row pillar adjacent to the first-panel end started to decrease immediately after the starting of mining and continued to fluctuate until the face had advanced 200 ft; then, the loading leveled off at slightly higher than the premining level. Between 200- and 400-ft face advances, this

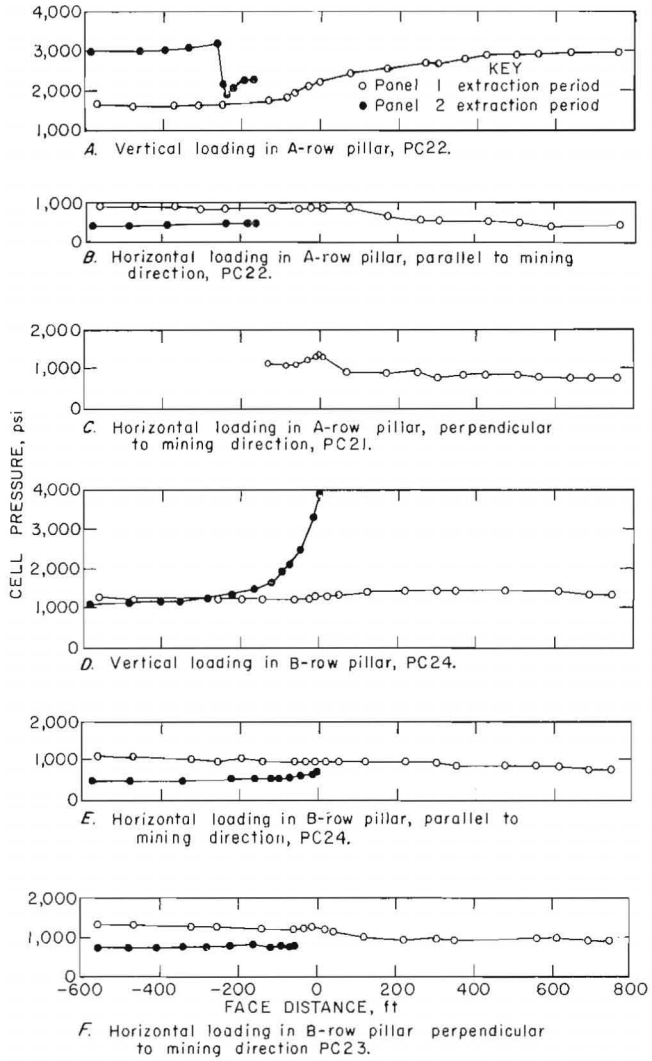

FIGURE 13. - Loading history of gate-entry pillars.

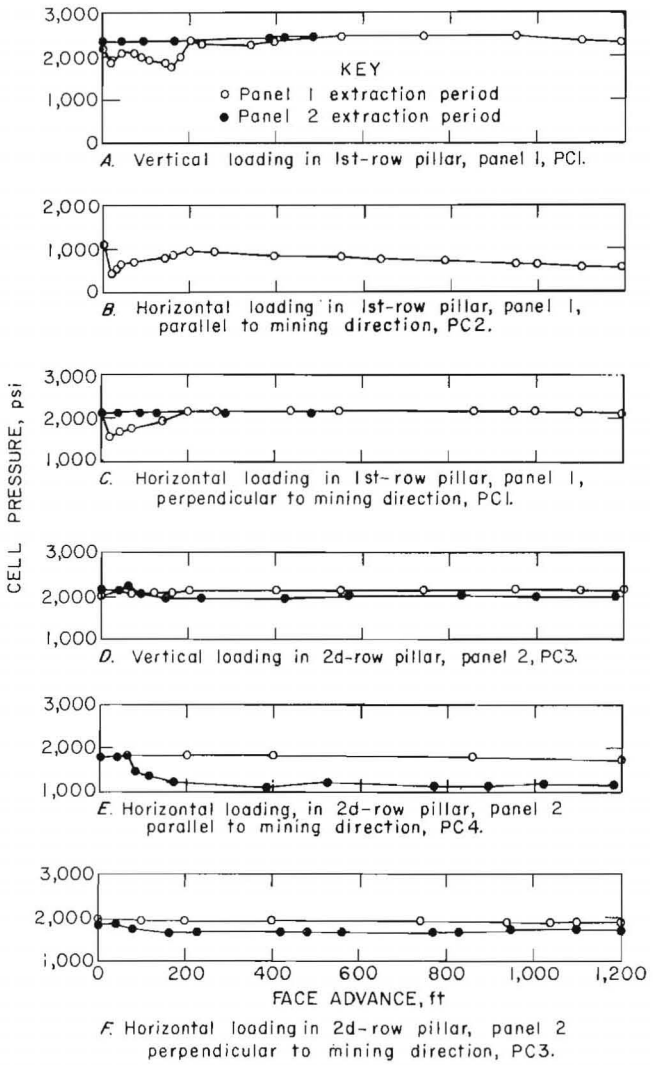

FIGURE 14. - Loading history of bleeder-entry pillars at panel starting ends.

vertical stress fluctuated again with much reduced amplitude. These phenomena may imply that the initial break of main roof over the panel occurred at 200-ft face advance and the second major break at 400-ft face advance. The second panel extraction caused only a slight increase in the loading of this same pillar, as shown in figure 14*A*, and may indicate that a portion of the overburden load was transferred back onto the first-panel gob.

Horizontal stress acting in the direction of mining in the first-row pillar at the end of panel 1 showed a major unloading-and-loading cycle during the period of the first 200-ft advance of the panel 1, and then continued a gradual unloading trend until it leveled off at its 50 pct magnitude (fig. 14*B*). Horizontal stress acting in the direction perpendicular to the direction of mining in the first-row pillar at the panel 1 end also indicated a major unloading-and-loading cycle during the first 200-ft face advance of panel 1, and then stabilized at the premining level of loading. The second panel (panel 2) extraction did not affect the horizontal loading of this pillar along the direction perpendicular to the direction of mining (fig. 14*C*).

The premining vertical loading of the second-row pillars at the starting end of panel 2 was approximately 10 pct lower than that of the first-row pillars. This loading suffered only a minor fluctuation caused by the panel 1 extraction up to 200 ft, then remained at approximately 10 pct higher level. The panel 2 extraction also caused a minor fluctuation to this pillar loading up to 200-ft face advance, then stayed at the premining level (fig. 14*D*).

Horizontal loading of the same pillar in the direction of mining showed no influence of the panel 1 extraction but indicated a significant unloading effect of the panel 2 extraction, starting from 60-ft face advance and ended at 200-ft face advance, then remained at 33 pct lower than the premining loading level (fig. 14*E*).

Horizontal loading of the same pillar in the direction perpendicular to the direction of mining showed no influence of the panel 1 extraction. A slight unloading effect of the panel 2 extraction, however, appeared at 40-ft face advance, continued up to 200-ft face advance, then remained at 10 pct lower than the premining level as shown in figure 14*F*.

Finishing-End Pillars

The relative position of the finishing-end bleeder-entry pillars differs from that of the starting-end bleeder-entry pillars because there was a 100-ft-wide barrier pillar left between the panel-end and the first-row pillars after the panel extraction was finished (fig. 1). Therefore only the effects of the panel extraction on the pillar loading of the immediate panel were significant and those of the neighboring panel extraction were negligible.

The loading histories of the finishing-end pillars are somewhat similar to the mirror images of those of the starting-end pillars. Those of the first (near) row pillars indicate unloading trends, whereas those of the second (far) row pillars indicate loading trends (fig. 15). This trend of loading histories, as indicated by figures 14 and 15, reveals that the abutment pressures at the end of panel had been shifted from the pillars in the first row to the second row after starting and before finishing of the panel extraction.

Reduction of load on the first-row pillars in vertical and in two horizontal directions started when the remaining panel length was approximately 800 ft. The vertical-pressure reduction of approximately 10 pct is shown in figure 15*A*. The horizontal pressure reduction in the mining direction amounted to 33

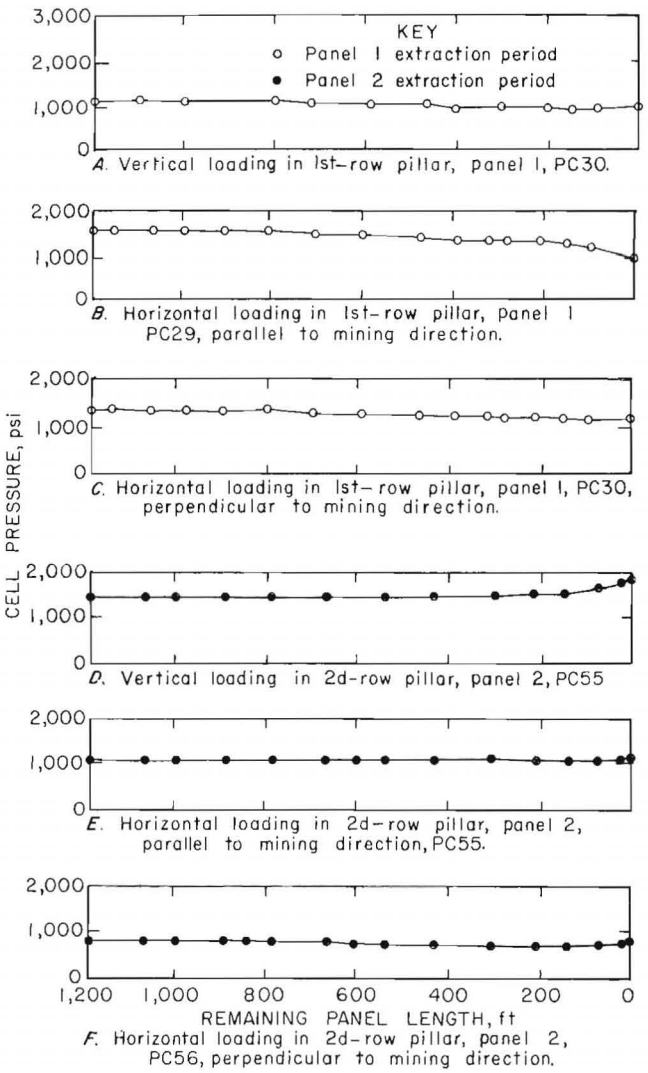

FIGURE 15. - Loading history of bleeder-entry pillars at panel finishing ends.

pct (fig. 15*B*); likewise the horizontal-pressure reduction in the direction perpendicular to mining direction amounted to 15 pct (fig. 15*C*).

Load transfer on the second-row pillars at the finishing end of panel 2 in the vertical direction and in the horizontal direction perpendicular to the mining direction started when the remaining panel length was approximately 200 ft and resulted in approximately a 20-pct increase, as shown in figure 15(*D* and *F*). The horizontal loading of the same pillar in the direction of mining was only slightly affected by the panel extraction, as shown in figure 15*E*.

Barrier Pillars

In barrier pillars for panels 1 and 2, the increase in vertical pressure and decrease in horizontal pressure appeared when the longwall face had approached to within the last 100-ft portion (figs. 16-17). The changes are 4 to 5 pct at all locations in the pillar. However, the premining pressures differ from location to location. Apparently, the highest vertical pressure at the edge of each pillar is due to the effect of side abutment pressure. The lowest horizontal pressure at the edge of each pillar is due to fracturing of that portion. After panel extraction was complete, the barrier pillar edges continued to fail because the increase of vertical pressure and the decrease of horizontal pressure continued, as indicated by PC34 and PC51 curves in figures 16 and 17.

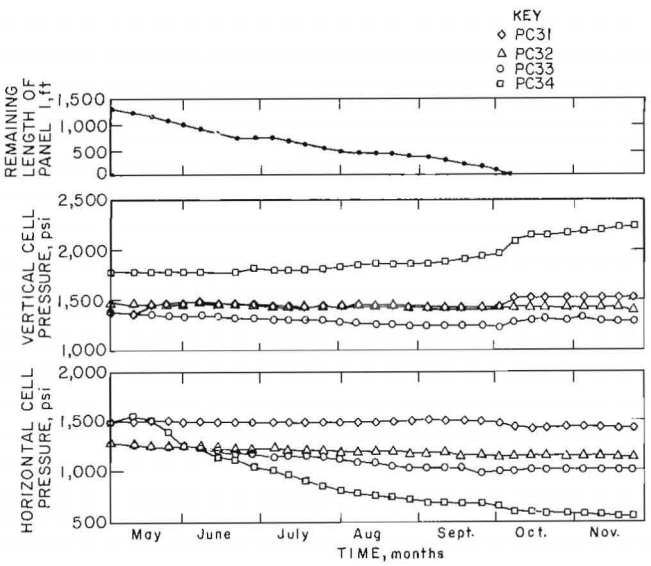

FIGURE 16. - Loading history of panel 1 barrier pillar.

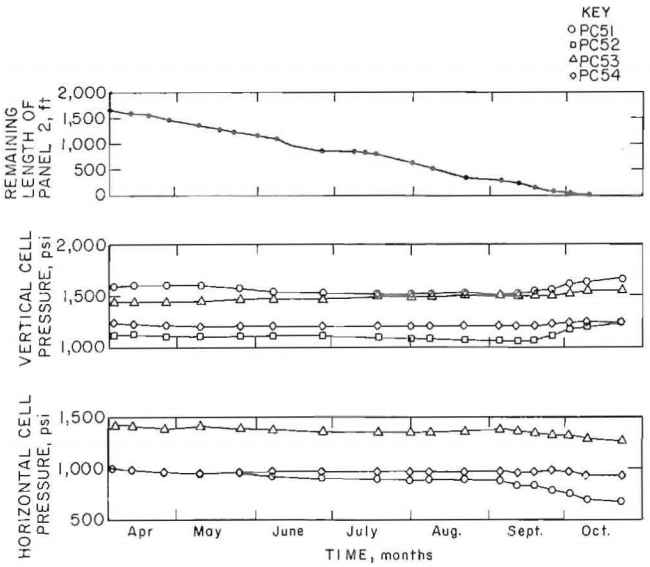

FIGURE 17. - Loading history of panel 2 barrier pillar.

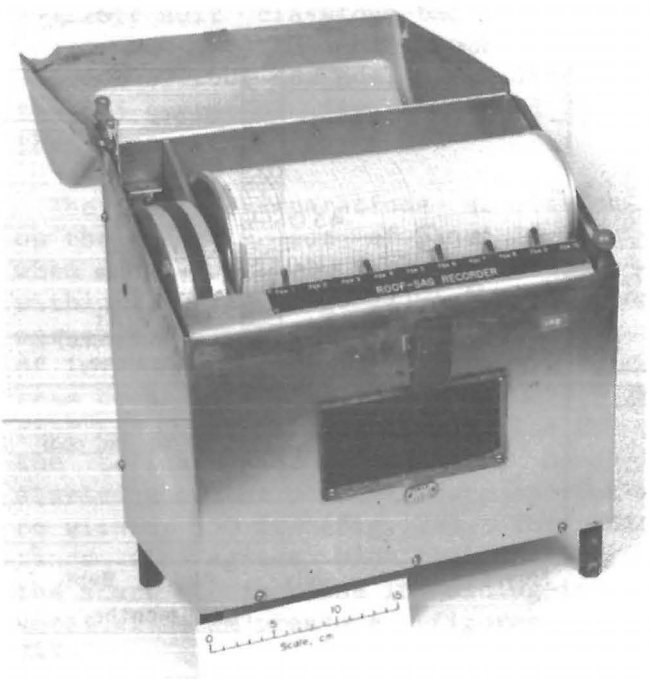

FIGURE 18. - Ten-anchor-point extensometer.

STRATA MOVEMENTS

DIFFERENTIAL ROOF-STRATA MOVEMENT AND BED SEPARATION

The mining-induced differential movements in roof strata and the bed separations were monitored by 10-point extensometers (fig. 18) installed in 3-in-diam vertical holes at stations R1, R2, and R3 shown in figure 6. The extensometer consisted of flat wedge-type anchors, 0.041-in-diam steel wires, and a spring-loaded, 7-day clock, 10-channel strip-chart recorder. The anchor depth varied from station to station: the deepest anchor positions ranged from 70 to 80 ft, while the recorders were anchored at the 3.5-ft depth. The No. 0 anchor at 3.5 ft is used as the reference point because most of the premining movement of the roof surface and its vicinity had occurred before the instrumentation was installed.

Based on the extensometer data of station R2 at the intersection of middle entry and the crosscut, the roof-strata movements induced by panel 1 extraction started before the face was within 200 ft distance, and continued until completion of panel 1 extraction with the most active movements occurred around the passage of the face. There was a brief stabilization period, approximately 3 months, before the panel 2 extraction induced further movements, which occurred

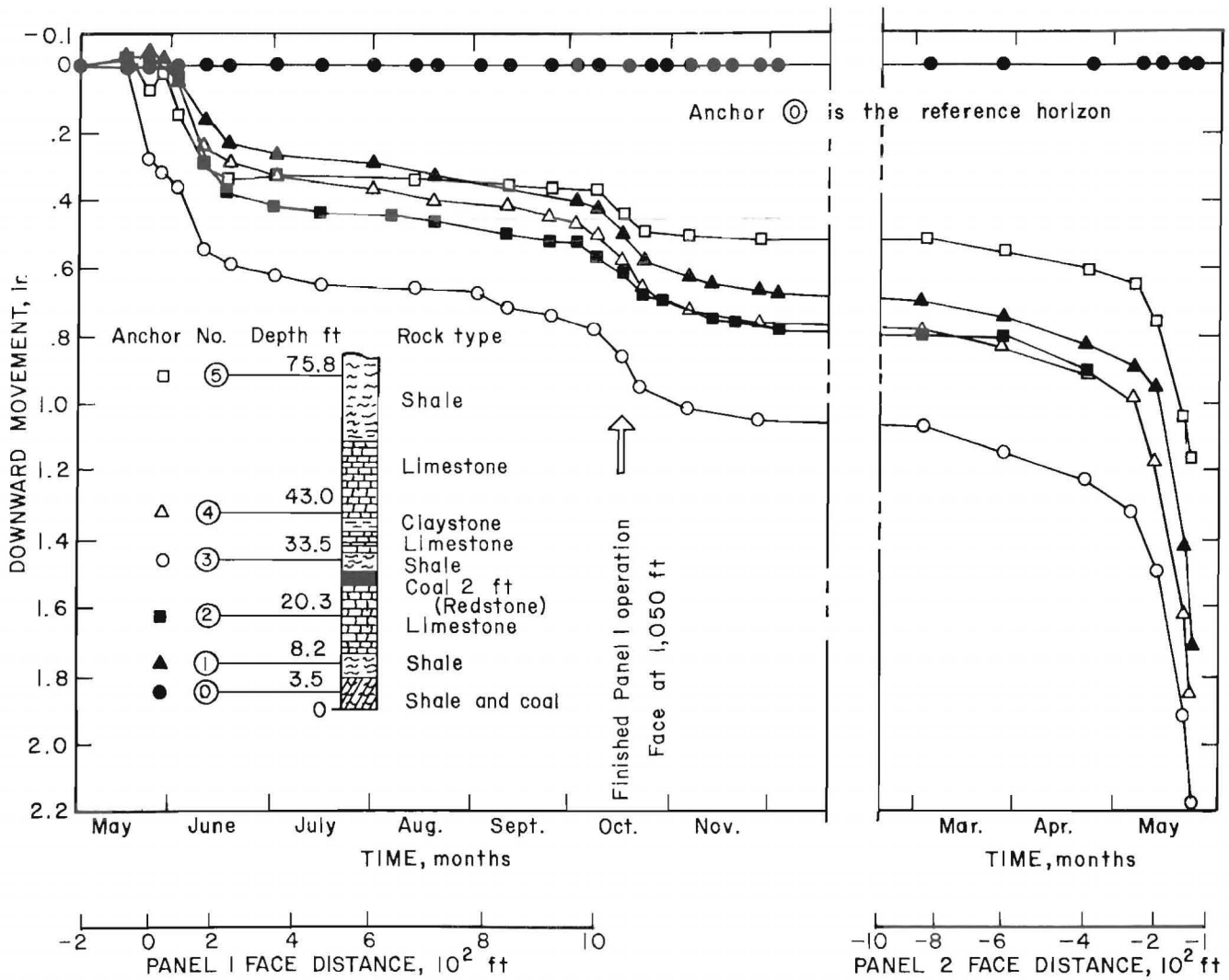

FIGURE 19. - Cumulative roof-strata movements at station R2.

at approximately -900-ft face distance and continued until the immediate roof (up to 40 ft) caved at approximately -100 ft of panel 2 face distance. The cumulative downward movement of the immediate roof, relative to the 75-ft horizon, exceeds 1.0 in, as indicated by figure 19 between anchors 3 and 5.

Roof-strata movements also occurred at the intersection of the first entry and the crosscut, station R1. The mining influence started before the panel 1 face had reached the -200-ft face distance, became more active at -120-ft face distance, and became very active at -50-ft face distance. The immediate roof over the station (28 ft and above) finally caved when the longwall face retreated 4 to 6 ft past the extensometer, as indicated in figure 20.

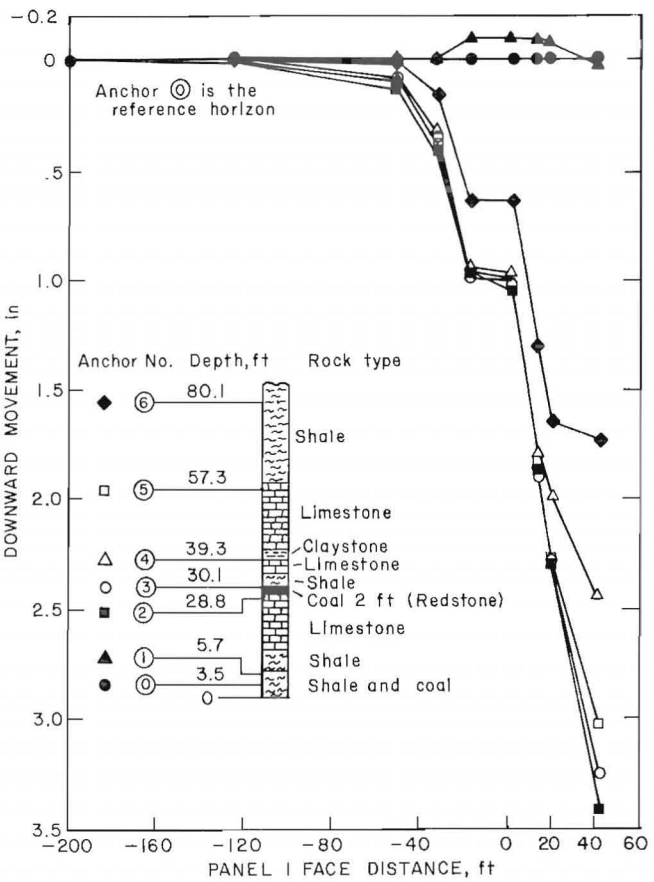

FIGURE 20. - Cumulative roof-strata movements at station R1.

Figure 21 shows the roof-strata movements that occurred at the intersection of the third entry and the crosscut, station R3. Measurement was started when the panel 1 face was at -23 ft from the extensometer. The roof strata movements started when the face passed 85 ft beyond the extensometer and stopped at 445-ft face distance. The effects of panel 2 extraction appeared when the face distance was -300 ft. The movements were accelerated at approximately -150-ft face distance. They reached the maximum rate at approximately -50-ft face distance. Then the roof caved at 15-ft face distance.

Three major roof-bed separation horizons were identified within 80 ft of the immediate roof strata; they are (1) the boundary between the shale-coal intercalating bed and shale bed, approximately 7 ft above the roof surface, as indicated by the 1-2 curve of figure 22 and 0-1 curves of figures 23 and 24, (2) the 4-ft, thinly bedded shale directly overlying the 2-ft Redstone seam, 30 ft above the roof surface, as indicated by the 3-4 curve of figure 22 and the 2-3 curves of figures 23 and 24, and (3) the 2-1/2-ft soft claystone bed between the upper and lower limestone beds, 40 ft above the roof surface, as indicated by the 4-5 curves of figures 22 and 24, and the 3-4 curve of figure 23.

The roof-bed separations at station R1 on the headgate side of panel 1 started when the panel 1 face approached to within 120 ft (fig. 22). This distance agrees with the distance at the start of increase in mining-induced vertical seam pressure (figures 10 and 22). The roof-bed separations at station R3 on the tailgate side of panel 2, however, started when the panel 2 face approached to within 150 ft (fig. 24). This distance also agrees with the distance at the start of increase in mining-induced vertical seam pressure (figures 11 and 24).

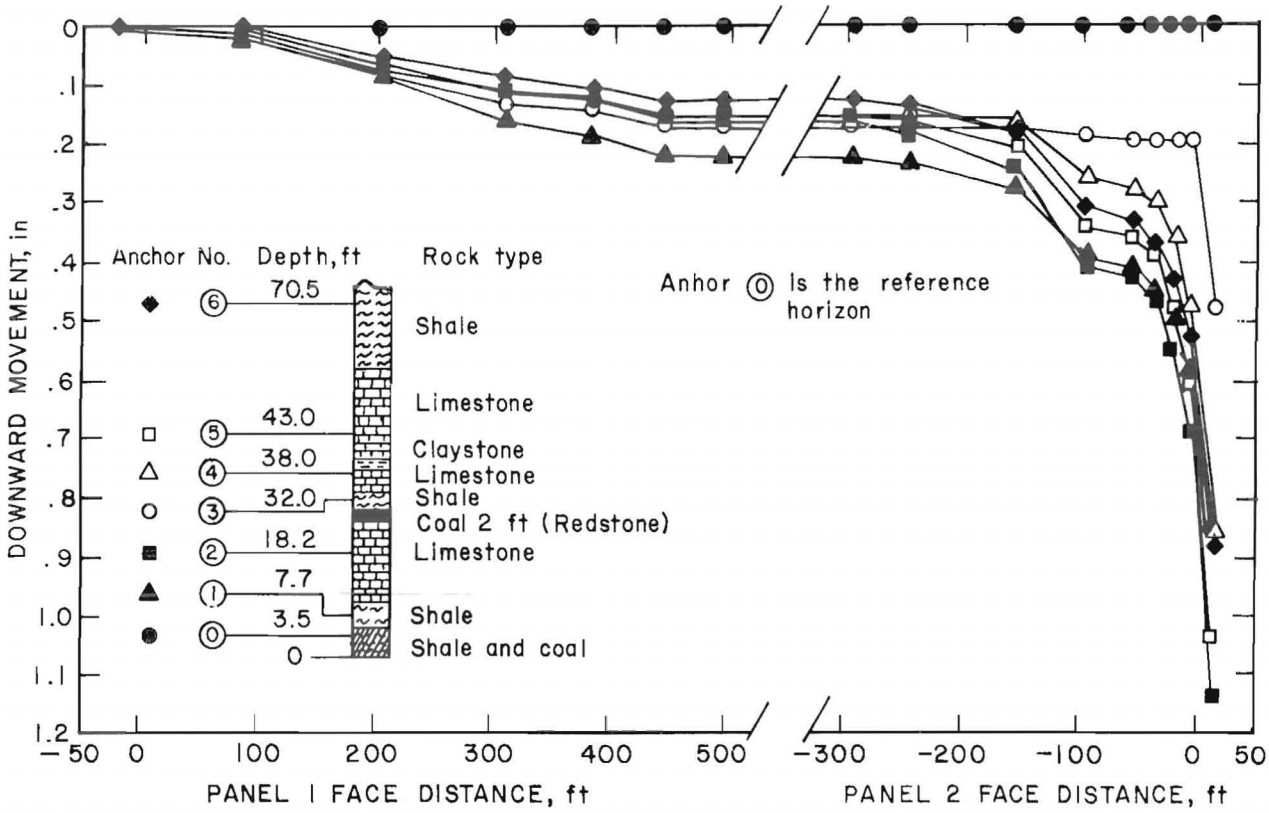

FIGURE 21. - Cumulative roof-strata movements at station R3.

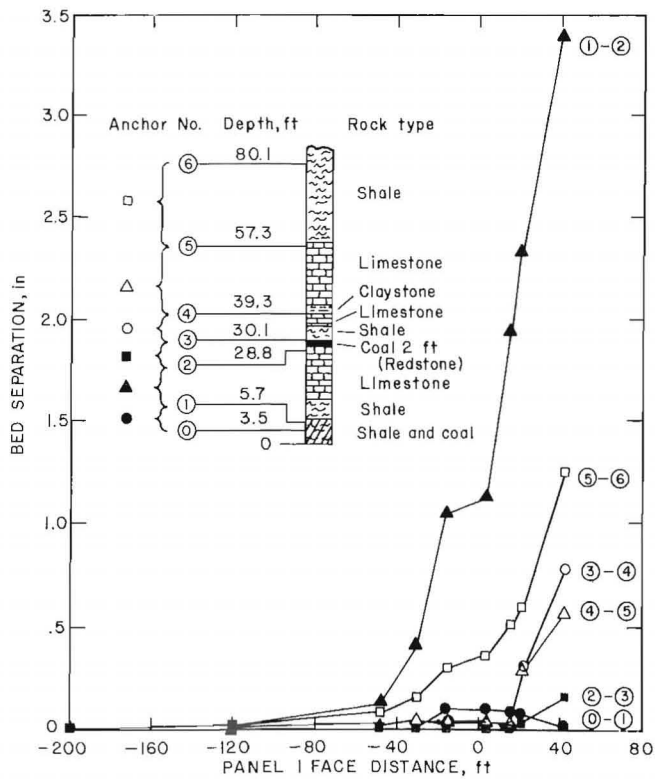

FIGURE 22. - Bed separations at station R1.

DIFFERENTIAL FLOOR LIFT

Mining-induced differential floor lifts relative to 18-in-deep roof horizon were measured at the three intersections of the three gate entries and a crosscut, as indicated by F1, F2, and F3 in figure 6. At each station, three 1-in-diam galvanized steel riser pipes were anchored at 3-, 7-, and 15-ft depths through 2.125-in-diam holes, as shown in figures 25, 26, and 27. A cap was placed on the top of the pipe and a small indentation was punched in the center to establish a fixed reference point. A 2-in-diam, 12-in-long galvanized collar pipe was then driven into the upper portion of the hole to protect the riser pipe. A cap was also placed on the 2-in pipe to keep dirt and water away from the riser pipe. Right above each riser pipe, a 0.75-in-diam roof bolt was anchored to 18-in depth in the roof. The bolt head was countersunk to fit the pointed end of a telescopic measuring rod. All installations except one operated satisfactorily throughout the period of this

investigation. The 3-ft installation at station F2 was destroyed by the supply tractor.

The data indicate that the magnitude of differential floor lift follows the depth of measuring strata; namely, in the descending order of 3-, 7-, and 15-ft depths. At station F1 (fig. 25), the panel 1 extraction-induced lift first occurred at -265-ft face distance, accelerated at -145-ft face distance, and reached the peak of 1.3 to 2.5 in at -5- to -3-ft face distances. At station F2

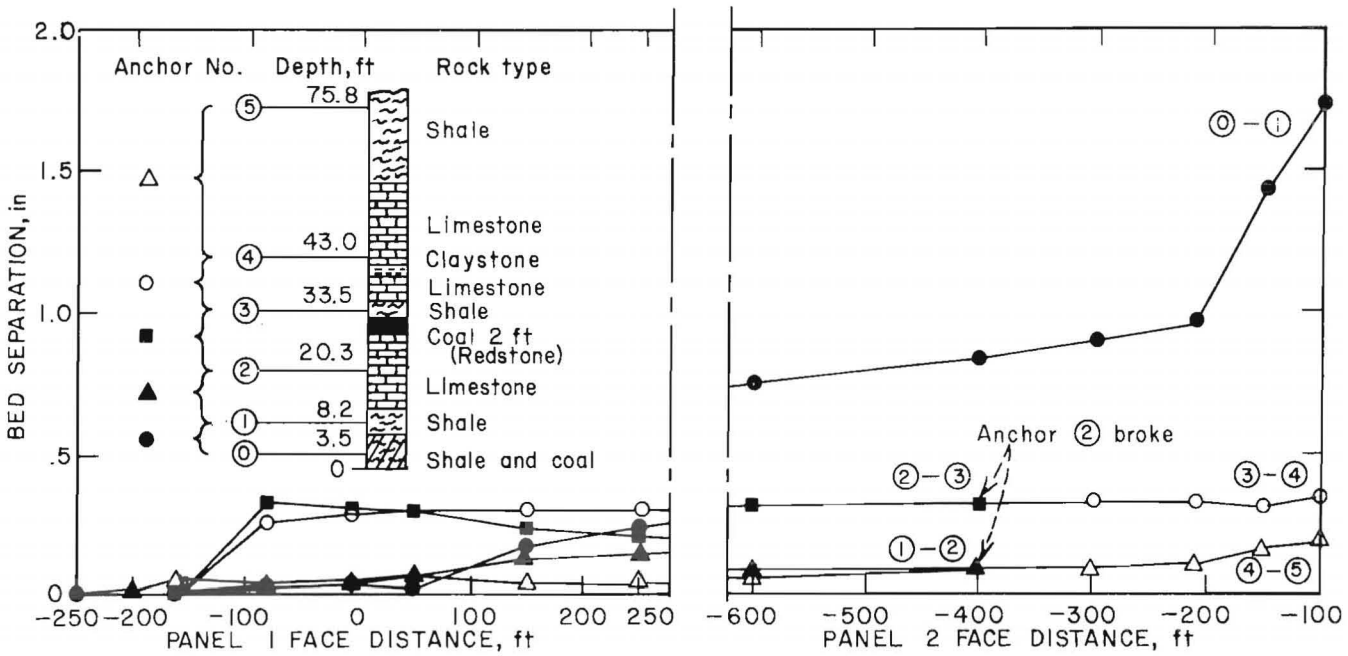

FIGURE 23. - Bed separations at station R2.

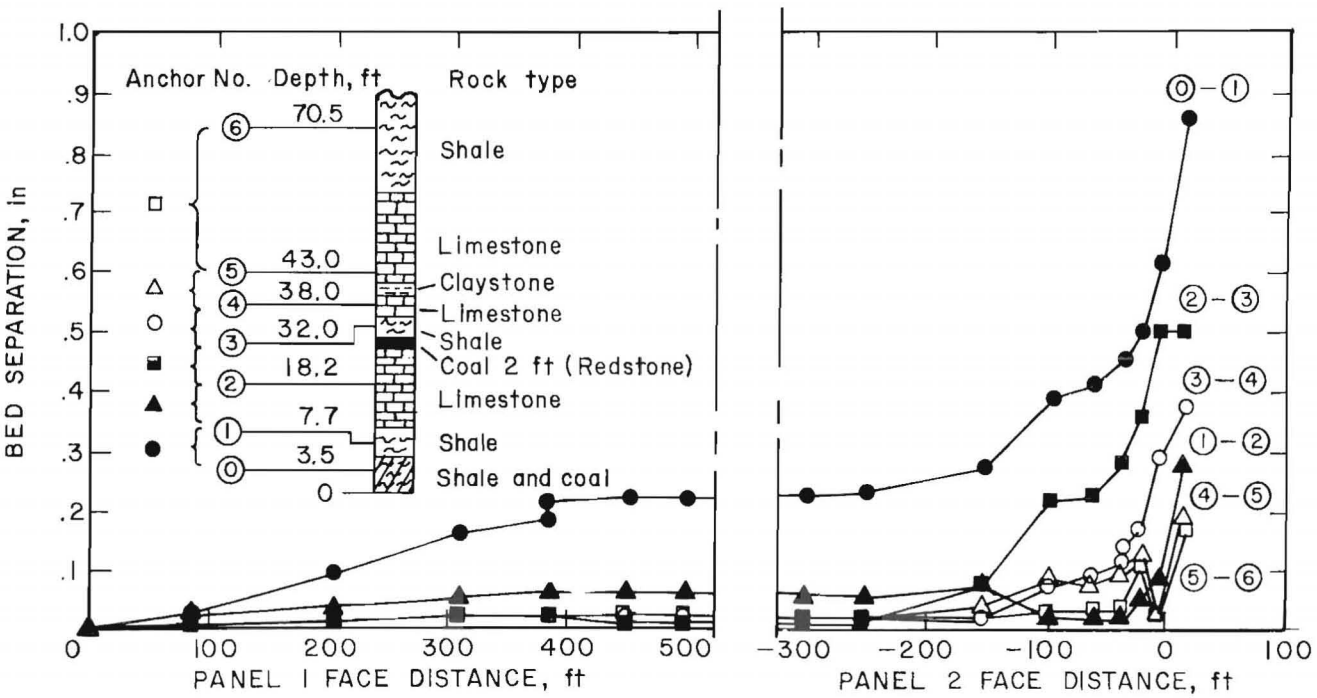

FIGURE 24. - Bed separations at station R3.

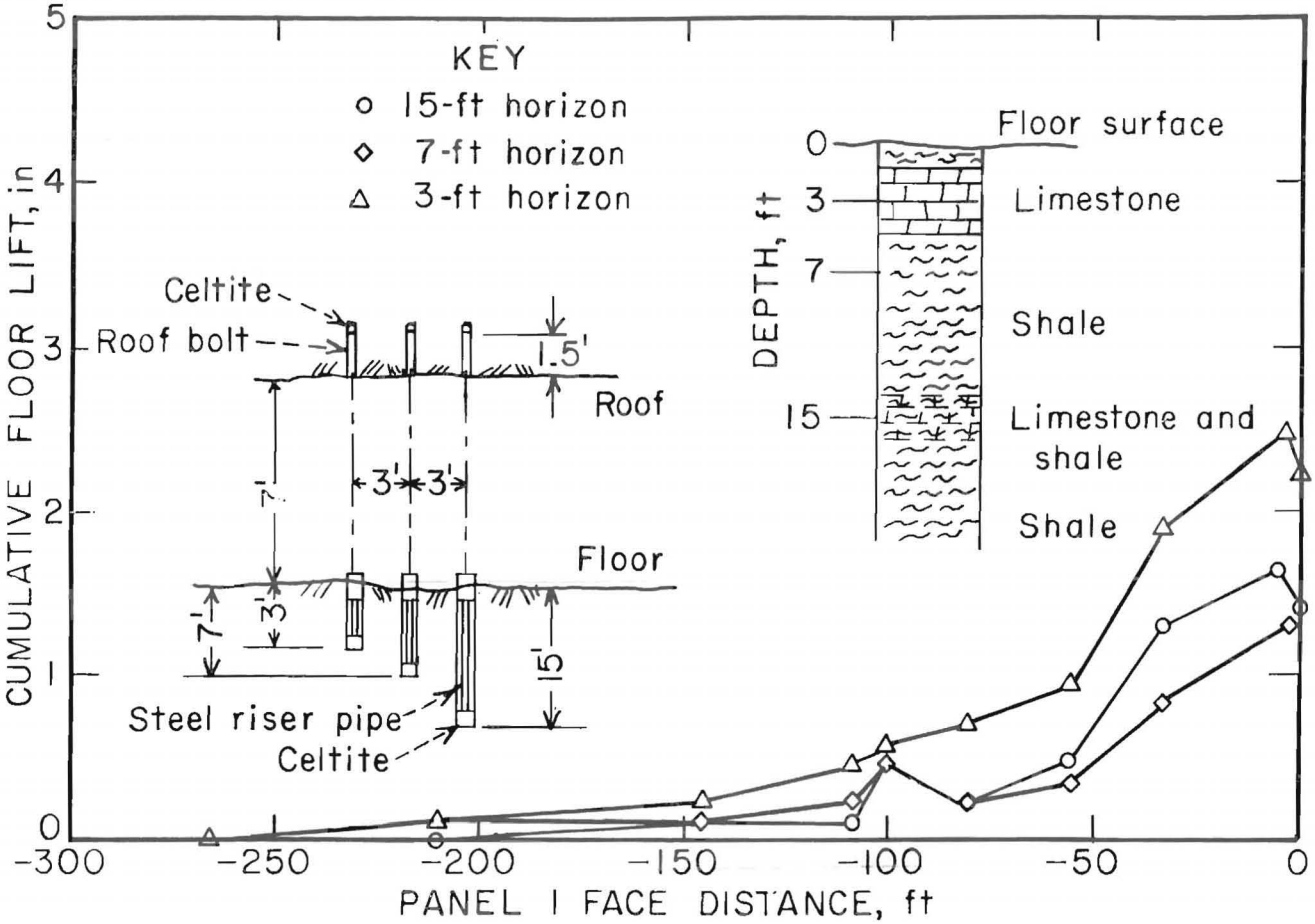

FIGURE 25. - Relative floor lift at station F1.

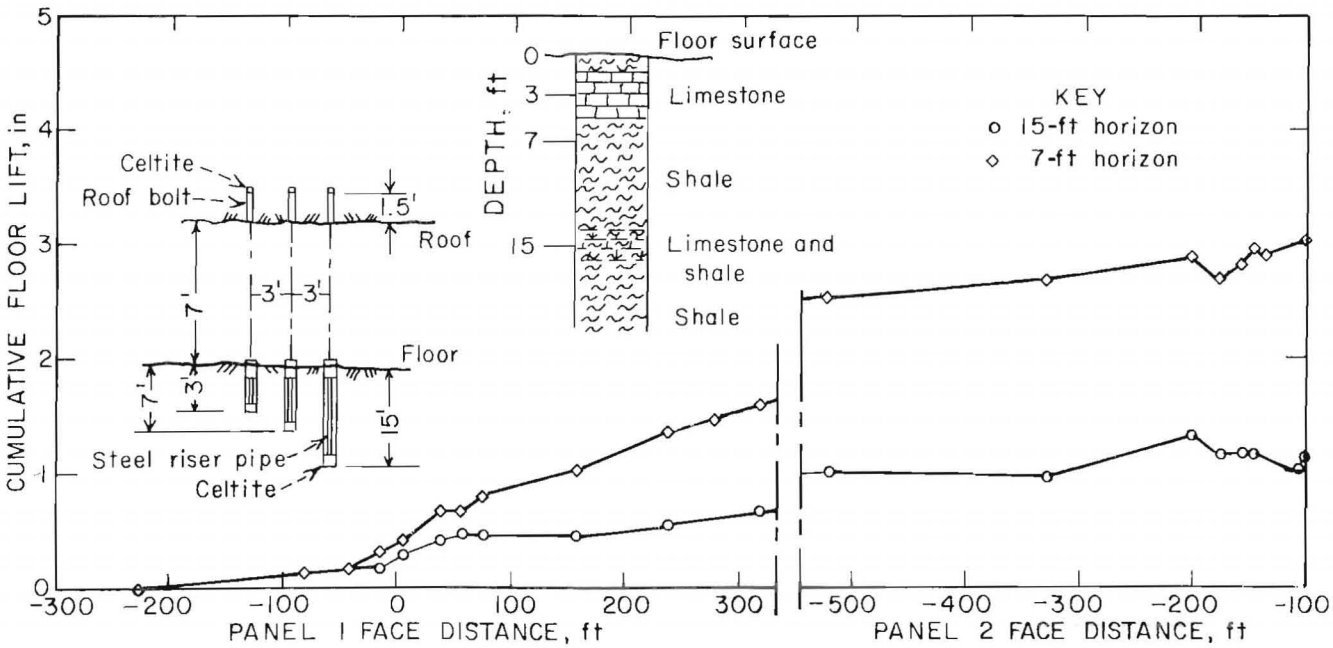

FIGURE 26. - Relative floor lift at station F2.

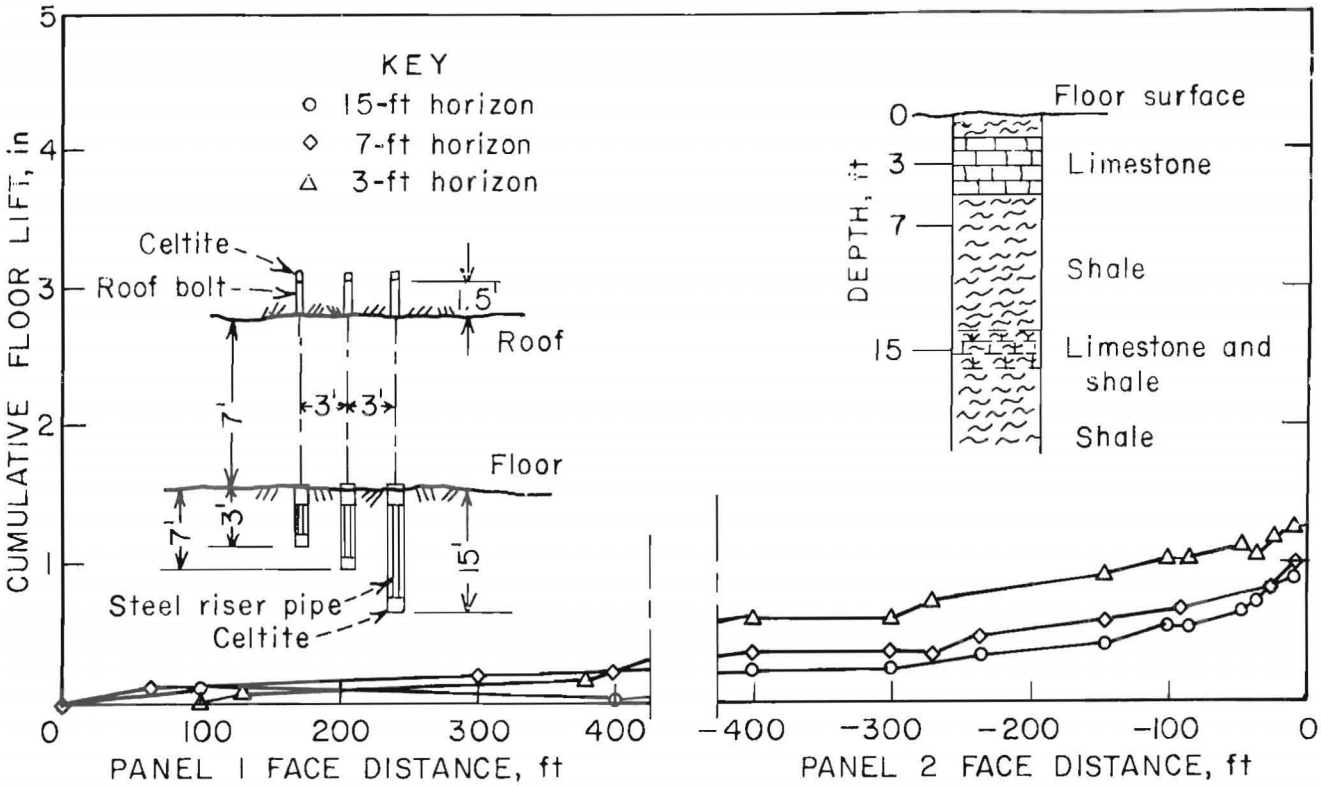

FIGURE 27. - Relative floor lift at station F3.

FIGURE 28. - Convergence recorder.

(fig. 26), the lift induced by the panel 1 extraction first appeared at -225-ft face distance, accelerated at -40-ft face distance, and continued to approximately 350-ft face distance. The lift induced by mining panel 2 at station F2, however, occurred at -330 ft and reached 3 in maximum lift (7-ft horizon) at -100-ft face distance when the station was destroyed by caving. At station F3 (fig. 27), the lift induced by mining panel 1 was found insignificant, the lift induced by mining panel 2 first occurred at -300-ft face distance, accelerated at -150-ft face distance, and then reached the maximum of 1 to 1.25 inch at -3-ft face distance, when the station was destroyed.

ENTRY ROOF-TO-FLOOR CONVERGENCE

Mining-induced roof-to-floor convergences were measured in the head entry of panel 1 (station CR1) and in the tail entry of panel 2 (station CR2), as shown in figure 6. The spring-wound clock convergence recorders (figs. 28-29) were set 3 ft away from the rib of the longwall panels. The roof and floor anchors for the recorders consisted of rock bolts in which the heads were machine grooved to allow a snug fit for recorder posts. All roof bolts were anchored at 1.5 ft depth, but the floor bolts were anchored at 1.5-ft and 4-ft depths for each station.

Measurements are plotted in figures 30 (station CR1) and 31 (station CR2). At both stations, the anchor at 4-ft depth into floor showed more convergence than the anchor at 1.5-ft depth. This is

because more floor lift of 1.5-ft horizon than that of 4-ft horizon had already occurred prior to the inception of mining-induced floor lift and convergence. Active mining-induced convergence appeared at approximately -150-ft face distance at both stations. The magnitude of convergence is rather small compared with the magnitude of floor lift at nearby stations because the convergence stations were set close to the rib of longwall panels (only 3 ft from the rib line).

SUMMARY AND CONCLUSIONS

This report summarizes a portion of the results of a comprehensive ground control study conducted at a mechanized longwall coal mine in West Virginia. The objective of this study was to develop simple and practical techniques of field measurement for ground control parameters. Special emphasis was placed on ground pressures, strata movements, and geomechanical properties. Significant findings are summarized as follows.

FIGURE 29. - Convergence meter.

- Bureau of Mines hydraulic borehole pressure cells, including the cylindrical (CPC) and flat (BPC) cells, are simple and efficient instruments to measure existing ground pressures, and to monitor mining-induced ground-pressure changes.

- Premining profile of vertical ground pressure across each panel is maximum at approximately 20 pct of the panel width inside the ribs. This phenomenon may suggest that a pressure arch was formed over the 210-ft-wide interpanel-entry system. Its abutments are at 20 pct of the panel width inside the ribs.

- The width of the vertical-front-pressure abutment in the longwall panel is approximately 0.18 to 0.20 times the average overburden thickness, including the yielded zone approximately equaling the extraction height.

- The idealized profile of vertical-front-abutment pressure across the panel, which was composed of data from the two panels, is unsymmetrical about the central axis. The skewness is amplified when the longwall face has approached the pressure cells. The central one-third of the panel shows the lowest abutment pressure. The gob-side abutment pressure is 2 to 3 times greater than that of the solid side because of the interaction of side-abutment pressures of the gate entries. The side-abutment pressure of the

tailgate entry is much higher than that of the headgate entry.

- The width of the front abutment and the magnitude of the vertical pressure can be used as criteria for entry support design. For that portion of entry where the front-abutment pressure occurs, the support density should be increased in proportion to the increase in the abutment pressure. Such support reinforcement may be achieved by adding cribs or hydraulic props.

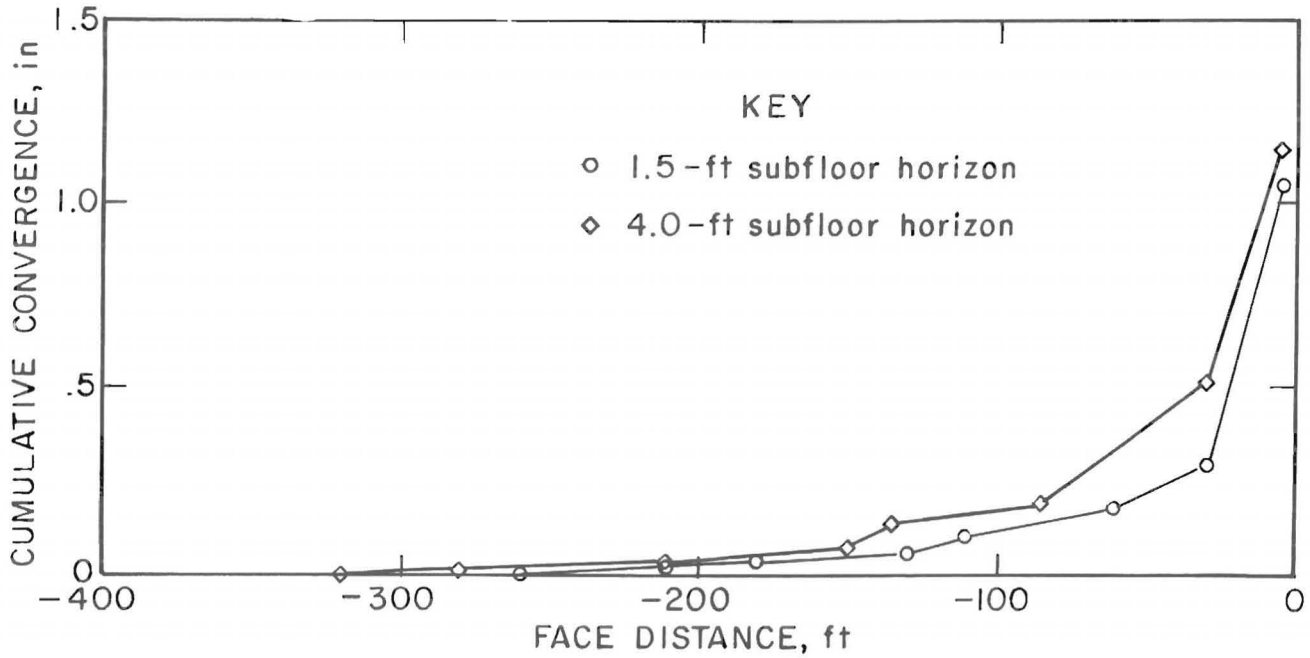

FIGURE 30. - Roof-to-floor convergence at station CR1.

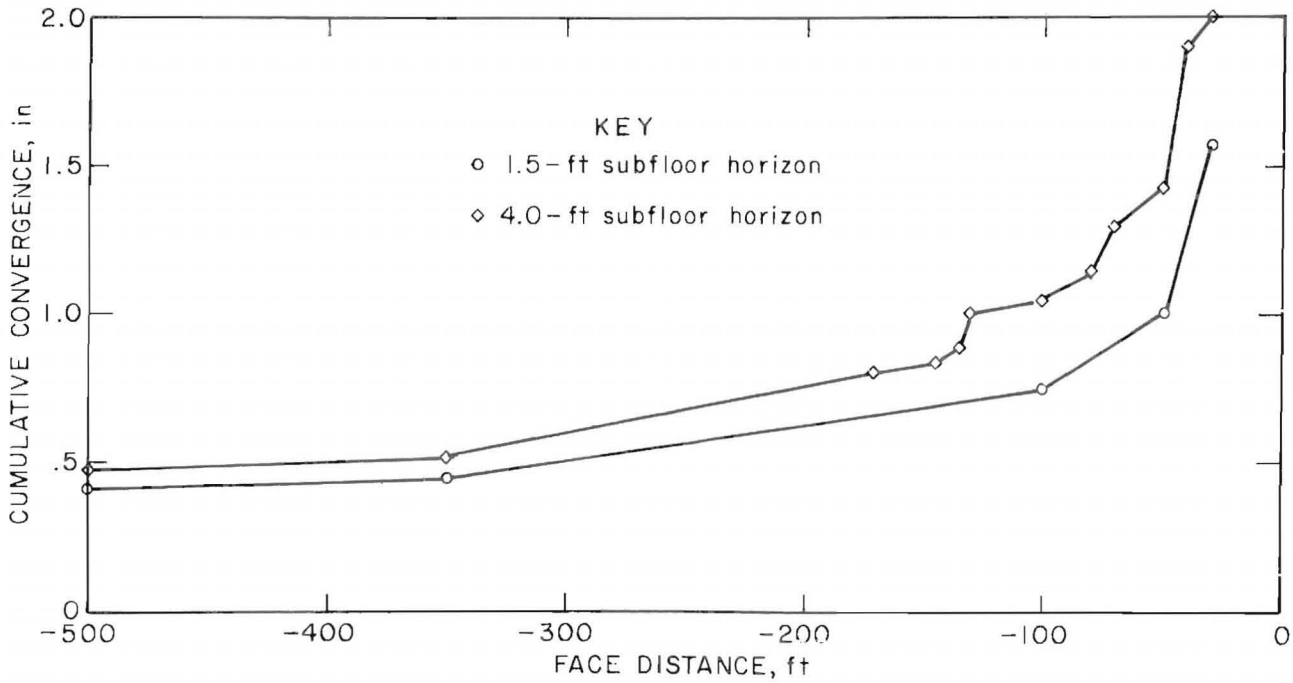

FIGURE 31. - Roof-to-floor convergence at station CR2.

- Vertical loading in the gate-entry pillars received the initial effects of extracting the immediate panel at -300-ft face distance (negative distance indicates that the instrumentation plane is in the solid area). The rate of increase was intensified at -100-ft face distance. The increase in the headgate entry pillars continued to the point beyond zero face distance. However, the load increase in the tailgate entry pillars peaked at zero face distance.

- Loading histories of the starting-end bleeder-entry pillars reveal that the initial break of the main roof over the panel may have occurred at 200-ft face advance, and the second break at 400-ft face advance, or that the main roof over the panel may have broken at approximately 200-ft intervals of longwall advance.

- The 10-anchor-point extensometer was an efficient instrument for monitoring the differential roof-strata movements and roof-bed separations, even if its installation was tedious.

- Three major roof-bed separation horizons were identified above the coal seam: (1) the boundary between the shale-coal intercalating bed and shale bed, which is approximately 7 ft above the roof surface, (2) the 4 ft of thinly bedded shale directly overlying the 2-ft Redstone seam, which is 30 ft above the roof surface, and (3) the 2-1/2-ft soft claystone bed between the upper and lower limestone beds, which is 40 ft above the roof surface.

- Active mining-induced roof-bed separations on the headgate-side of panel 1 started when the panel 1 longwall approached to within -120 ft. Those on the tailgate side of panel 2 started at -150-ft face distance. These distances agree closely with the distances at which the mining-induced vertical seam pressures started to increase.

- Magnitude of differential floor lift is in accordance with the depth of measured strata, specifically, in the descending order of 3-, 7-, and 15-ft depths. The lift induced by panel extraction first occurred at -225- to -300-ft face distance, accelerated at -145- to -150-ft face distance, and reached the peak at -3- to -5-ft face distance.

In conclusion, some simple and practical investigations of ground control before and during the longwall operation is essential to the success of mechanized longwall operations. The techniques and instrumentation layout presented in this report can be used as guidelines for such studies.

REFERENCES

1. Harza Engineering Co. Comprehensive Ground Control Study of a Mechanized Longwall Operation. Final report (contract H0230012). BuMines OFR 5(1)-77, 1976, 151 pp.; OFR 5(2)-77, 1976, 270 pp.; NTIS PB 262-475, 476.

2. Lu, P. H. Stability Evaluation of Retreating Longwall Chain Pillars With Regressive Integrity Factors. Pres. at the 5th International Congress on Rock Mechanics (Melbourne, Australia, Apr. 10-15, 1983). A. A. Balkema, Rotterdam, Netherlands, v. 2, 1984, pp. E37-E40.

3. Panek, L. A., E. E. Hornsey, and R. L. Lappi. Determination of the Modulus of Rigidity of Rock by Expanding a Cylindrical Pressure Cell in a Drillhole. Proceedings, 6th U.S. Symposium on Rock Mechanics, Rolla, MO, Oct. 1964, pp. 427-449; available upon request from P. H. Lu, BuMines, Denver, CO.

4. Lu, P. H. Determination of Ground Pressure Existing in a Viscoelastic Rock Mass by Use of Hydraulic Borehole Pressure Cells. Pres. at the International Society for Rock Mechanics Symposium on Weak Rock (Tokyo, Japan, Sept. 21-24, 1981). A. A. Balkema, Rotterdam, Netherlands, v. 1, 1981, pp. 459-465.

5. _____. Mining-Induced Stress Measurement With Hydraulic Borehole Pressure Cells. Pres. at the 25th U.S. Symposium on Rock Mechanics (Evanston, IL, June 25-27, 1984). Soc. Min. Eng., AIME, Littleton, CO, 1984, pp. 204-211.

6. Griggs, D. T. Creep of Rocks. J. Geol., v. 47, 1939, pp. 225-251.

7. Flügge, W. Viscoelastic Beams. Ch. in Viscoelasticity. Blaisdell Publ. Co., London, 1967, pp. 32-33.

APPENDIX A.--THEORETICAL CONSIDERATIONS FOR DETERMINATION OF GROUND PRESSURE EXISTING IN A VISCOELASTIC ROCK MASS BY USE OF HYDRAULIC BOREHOLE PRESSURE CELLS[1]

BASIC PRINCIPLES

The state of stress in an in situ intact rock mass, whether it is homogeneous or heterogeneous, isotropic or anisotropic, and elastic or inelastic, is initially in equilibrium or inactive. However, once a hole is drilled into such a rock mass, the ground pressure existing in the vicinity of the hole will become active due to stress relief of the portion of the hole.

Usually, most geologic materials are elastic, but some of them may show time effects such as creep under an intermediate (compared with the breaking strength of rock) constant stress (6). However, the general problem of stress-strain analysis is the same for elastic and for viscoelastic structures. The only difference is that for viscoelastic structures, Hooke's law is to be replaced by a viscoelastic stress-strain relationship derived from creep. In other words, the viscoelastic solutions can be derived from those of the elastic problem by replacing the elastic modulus with the viscoelastic modulus on the basis of the elastic-viscoelastic correspondence principle (7).

In the case of a long drill hole in a viscoelastic, deep rock formation, loads are imposed by external biaxial (e.g., vertical and horizontal) ground pressures and, simultaneously, by internal dilating pressure introduced by the pressure cell. The state of stress in the rock mass is the same as that in an elastic rock under the same loading condition, but the associated displacements and strains are time dependent. The solution to the problem can be derived from the elastic theory for a problem of the same geometry and subjected to the same boundary loads. If the viscoelastic effects appear in a linear manner, substitute the corresponding viscoelastic modulus (or the reciprocal of the creep compliance) for the elastic modulus, which is based on the correspondence principle between viscoelastic and elastic theories. Poisson's ratio may be assumed as time independent. In fact, the time dependency and the variance of Poisson's ratio are both insignificant compared with the viscoelastic modulus for most types of rock.

SUM OF BIAXIAL GROUND PRESSURES

Based on the "principle of superposition," the problem of the radial displacement of a long drill hole at depth in a uniform elastic rock formation, subjected to an internal pressure P_i can be resolved into the problems of an infinite plate with a circular center hole subjected to a biaxial stress field, and of a thick-wall cylinder with an infinite outer radius and subjected to an internal pressure P_i, as shown in figure A-1.

For an infinite plate with a circular center hole subjected to a biaxial stress field, under the special plane strain condition in which the axial strain is zero ($\varepsilon_z = 0$), the radial displacement U_{ao} at the periphery of the hole ($r = a$) is determined by

$$U_{ao} = \frac{a(1-\nu^2)}{E} [(N_1 + N_2) + 2 (N_1 - N_2) \cos 2\theta], \qquad (A-1)$$

[1]Excerpt of reference 4 (pp. 460-463).

where N_1 and N_2 are normal stresses acting at the infinite boundaries, r and θ are the polar coordinates of the point in consideration, E is the modulus of elasticity, and ν is Poisson's ratio. For an elastic and infinitely thickwalled cylinder subjected to an internal pressure P_i, the radial displacement U_{ai} on the inner wall of the cylinder (r = a) can be written as

$$U_{ai} = \frac{a(1+\nu)P_i}{E}. \qquad (A-2)$$

The net radial displacement U_a at the periphery of the hole, due to the ground pressures and the inner dilating fluid pressure, can be obtained by superimposing the two displacements U_{ao} and U_{ai}. Noting that U_{ao} and U_{ai} have opposite signs, then

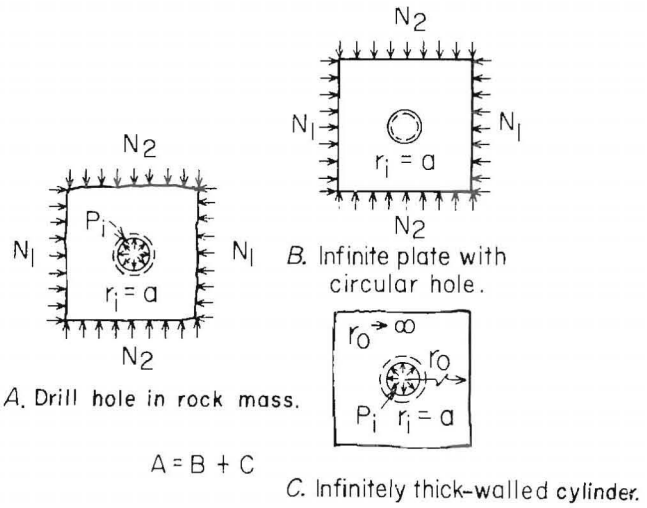

NOTE: Broken line indicates deformation.

FIGURE A-1. - Schematic of ground pressure in rock mass.

$$U_a = \frac{a(1+\nu)}{E}\left[P_i - (1-\nu)\{(N_1+N_2) + 2(N_1-N_2)\cos 2\theta\}\right]. \qquad (A-3)$$

Since U_a is a function of θ, the volume change V_d of the drill hole within the active length L due to the ground pressure and the inner dilating fluid pressure induced by a cylindrical pressure cell can be expressed as

$$V_d = \frac{L}{2}\int_0^{2\pi}(a \pm U_a)^2\, d\theta - \pi a^2 L = \pm\frac{2\pi a^2 L(1+\nu)}{E}\{P_i - (1-\nu)(N_1+N_2)\}. \qquad (A-4)$$

By virtue of the correspondence principle, E in equation A-4 can be replaced with the reciprocal of creep compliance J(t), which is the function of time t for the viscoelastic case, by assuming that Poisson's ratio is time independent; thus we obtain the time-dependent volume change

$$V_d(t) = \pm 2\pi a^2 L(1+\nu)\{P_i(t) - (1-\nu)(N_1+N_2)\}J(t). \qquad (A-5)$$

On the other hand, when a cylindrical pressure cell is pressurized and expanded in a drill hole and the outer shell of the cell is made fully in contact with the wall of the drill hole, the following relationship exists between the two volume-pressure ratios V_d/P_d of the drill hole and V_c/P_c of the pressure cell:

$$V_d/P_d = K_1 + K_2\,(V_c/P_c) \quad \text{or} \quad -V_d = C\,P_d, \qquad (A-6)$$

where $C = K_1 + K_2\,(V_c/P_c)$, V_d is the volume change in the drill hole, V_c is the fluid volume change and P_c is the fluid pressure change in the pressure cell, K_1 is the constant determined by the compressibility of fluid body retained in the pressure cell, which has the negative value, and K_2 is the response ratio between drill hole and pressure cell, which is dependent on the bulk moduli or

compressibilities of the rock mass and the pressure cell. For the rock mass with the time-dependent properties,

$$-\dot{V}_d(t) = C\, P_d(t). \qquad (A\text{-}7)$$

From equations A-5 and A-7, we obtain the relationship between the biaxial ground pressures N_1, N_2, and the pressure change in the drill hole $P_d(t)$:

$$P_d(t) = \mp\, 2\,\pi\, a^2 L(1+\nu)\{P_i(t) - (1-\nu)(N_1 + N_2)\}J(t)/C. \qquad (A\text{-}8)$$

A drill hole subjected to external biaxial ground pressures and internal dilating pressure will tend to restore the strain equilibrium by means of stress compensation. If the stress is compensated to its original equilibrium state; namely, if $P_d(t) = 0$, then $V_d(t) = 0$. From equation A-8, we can see that if $N_1 + N_2 = P_i(t)/(1-\nu)$, then $P_d(t) = 0$ because in equation A-8, all terms but $\{P_i(t) - (1-\nu)(N_1 + N_2)\}$ are nonzero. If we replace the cell pressure $P_i(t)$ under such condition with P_e, which may be called equilibrium cell pressure, then

$$N_1 + N_2 = P_e/(1-\nu). \qquad (A\text{-}9)$$

If there is any cell for which the borehole strain is in equilibrium because the stress is in equilibrium at an arbitrary time t, namely, if $P_d(t) = 0$, then both $\dot{P}_d(t) = 0$ and $\dot{P}_i(t) = 0$. Consequently, we obtain $P_e = P_i(t)$ from equation A-10.

Thus the sum of the biaxial ground pressures $N_1 + N_2$ can be obtained from equation A-9 with a single pressure cell installation by taking the cell pressure reading $P_i(t)$ as P_e when $P_i(t)$ has leveled off as shown in figure A-2*A*.

If the multiple cells are installed at the same spot with different initial pressures (fig. A-2*B*), then we may compare the rates of cell pressure change to obtain the equilibrium cell pressure P_e during the early period of the test. By differentiating both sides of equation 8 with respect to t and substituting equation A-9, we obtain

$$\dot{P}_d(t) = \mp\, 2\pi a^2 L(1+\nu)J(t)[\dot{P}_i(t) + \{P_i(t) - P_e\}\dot{J}(t)/J(t)]/C. \qquad (A\text{-}10)$$

Thus the equilibrium cell pressure P_e can be found from the $\dot{P}_i(t)$ versus $P_i(t)$ graph for an arbitrary t (e.g., t = 10 days) as the $P_i(t)$-intercept of the regression line as shown in figure A-2*C*.

RATIO OF BIAXIAL GROUND PRESSURES

Field experiments showed that when an encapsulated flat borehole pressure cell (EBPC) is installed in a drill hole and pressurized, the directional displacement of the drill hole U(t) will occur proportionally to the difference between the internal pressure and the effective external pressure of the cell. Therefore, we have an empirical relationship

$$U(t) = [\bar{P}_i(t) - K\,N]\bar{J}(t), \qquad (A\text{-}11)$$

where $\bar{J}(t)$ is the composite compliance of rock mass, capsule material, and cell material, $\bar{P}_i(t)$ is the internal cell pressure, N is the resultant directional ground pressure, and K is the pressure response ratio that is dependent on the composite compliance of rock mass, capsule material, and cell material. Also, there is a relationship $\bar{P}_d(t) = k\,U(t)$ existing between U(t) and the pressure change at the inner wall of the drill hole $\bar{P}_d(t)$, where k is the proportionality constant; therefore, with substitution of equation A-11, we have

$$\bar{P}_d(t) = k\,[\bar{P}_i(t) - K\,N]\bar{J}(t). \qquad (A\text{-}12)$$

Equation A-12 indicates that

$\bar{P}_i(t) - K\,N = 0$ is a sufficient condition for $\bar{P}_d(t) = 0$.

To derive the rate of the pressure change in the drill hole, $\dot{\bar{P}}_d(t)$ for the short-term pressure convergence test with the multiple-EBPC installation, we differentiate both sides of equation A-12 with respect to t and obtain

$$\dot{\bar{P}}_d(t) = k\bar{J}(t)[\dot{\bar{P}}_i(t) + \{\bar{P}_i(t) - K\,N\}\,\dot{\bar{J}}(t)/\bar{J}(t)]. \qquad (A\text{-}13)$$

From this equation it is evident that $\bar{P}_i(t) - K\,N = 0$ is the condition for $\dot{\bar{P}}_d(t) = 0$, because when $\bar{P}_d(t) = 0$, both $\dot{\bar{P}}_d(t) = 0$ and $\dot{\bar{P}}_i(t) = 0$. In both cases, if we take the $\bar{P}_i(t)$ under the condition $\bar{P}_i(t) - K\,N = 0$ as the equilibrium cell pressure $\bar{P}_e$, we may write $\bar{P}_e = K\,N$. Then by knowing the equilibrium cell pressures in the two orthogonal directions $\bar{P}_{e1}$ and $\bar{P}_{e2}$, the ratio $Q = \bar{P}_{e1}/\bar{P}_{e2}$ can be expressed in terms of N_1 and N_2 as $Q = (N_1 + S\,N_2)/(N_2 + S\,N_1)$, where S is the transverse sensitivity of the flat borehole pressure cell body, which is equivalent to the ratio of effective cross-sectional areas in the two orthogonal directions. From this relationship, the ratio of the biaxial ground pressures can be derived as

$$N_1/N_2 = (Q - S)/(1 - Q\,S). \qquad (A\text{-}14)$$

The numerical value of S is 0.185 for the EBPC currently in use, calculated from the configuration of the cell body.

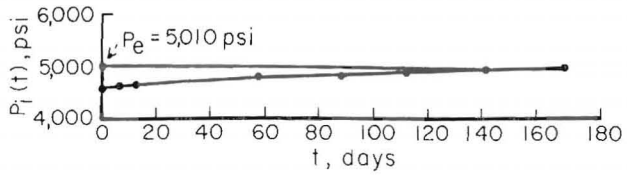

A. $p_i(t)$ vs t, long-term pressure convergence.

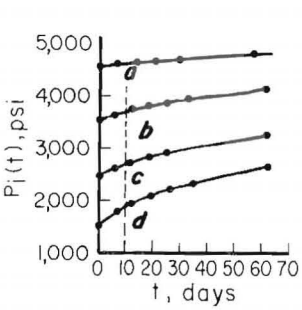

B. $p_i(t)$ vs t, short-term pressure convergence.

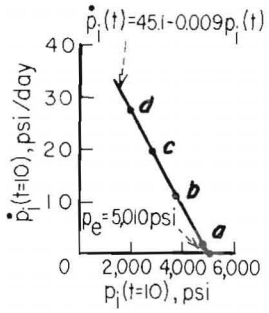

C. $\dot{p}_i(t)$ vs $p_i(t)$, short-term pressure convergence.

FIGURE A-2. - Procedure for determining CPC equilibrium pressure.

APPENDIX B.--BASIC CONCPETS OF MINING-INDUCED STRESS MEASUREMENT WITH HYDRAULIC BOREHOLE PRESSURE CELLS[1]

The magnitude of biaxial ground pressures existing in a rock mass can be determined by pressure convergence tests using a combination of one CPC and two preencapsulated flat BPC's installed in a single drill hole, as shown by figure B-1. Based on the elastic theories of plates and thick-walled cylinders, and by application of the elastic and viscoelastic correspondence principle, two equations were derived to calculate the biaxial stresses, N_1 and N_2, existing in a viscoelastic rock mass (4).

$$N_1 + N_2 = P_{e\text{-}CPC} / (1-\nu), \qquad (B\text{-}1)$$

$$N_1 / N_2 = (Q - S) / (1 - Q \times S), \qquad (B\text{-}2)$$

where $P_{e\text{-}CPC}$ is the equilibrium pressure of CPC (fig. B-2*A*), ν is Poisson's ratio of the rock mass, $Q = P_{e1} / P_{e2}$ where P_{e1} and P_{e2} are the equilibrium pressures of two BPC's (figure B-2*A*, $P_{e\text{-}BH}$ and $P_{e\text{-}BV}$), and S is the transverse sensitivity of the BPC, which is 0.185 as calculated from the geometry of the current Bureau of Mines cells.

Using the same rationale, the changes in the in situ biaxial ground stresses induced by mining or excavation can be determined with the same instrumentation (fig. B-1). If the biaxial stresses are vertical and horizontal pressures as shown in figure B-2, the two equations required are

$$N_H + N_V = P_{CPC} / (1-\nu), \qquad (B\text{-}3)$$

and

$$N_H / N_V = (Q - S) / (1 - Q \times S), \qquad (B\text{-}4)$$

where N_H and N_V are horizontal and vertical ground pressures respectively, P_{CPC} is the pressure reading of CPC, and $Q = P_{BH} / P_{BV}$, where P_{BH} and P_{BV} are horizontal and vertical BPC pressure readings, respectively (fig. B-2*A*). In this case, P_{CPC}, P_{BH}, and P_{BV} are equivalent to $P_{e\text{-}CPC}$, $P_{e\text{-}BH}$, and $P_{e\text{-}BV}$,

[1]Excerpt of reference 5 (pp. 205-207).

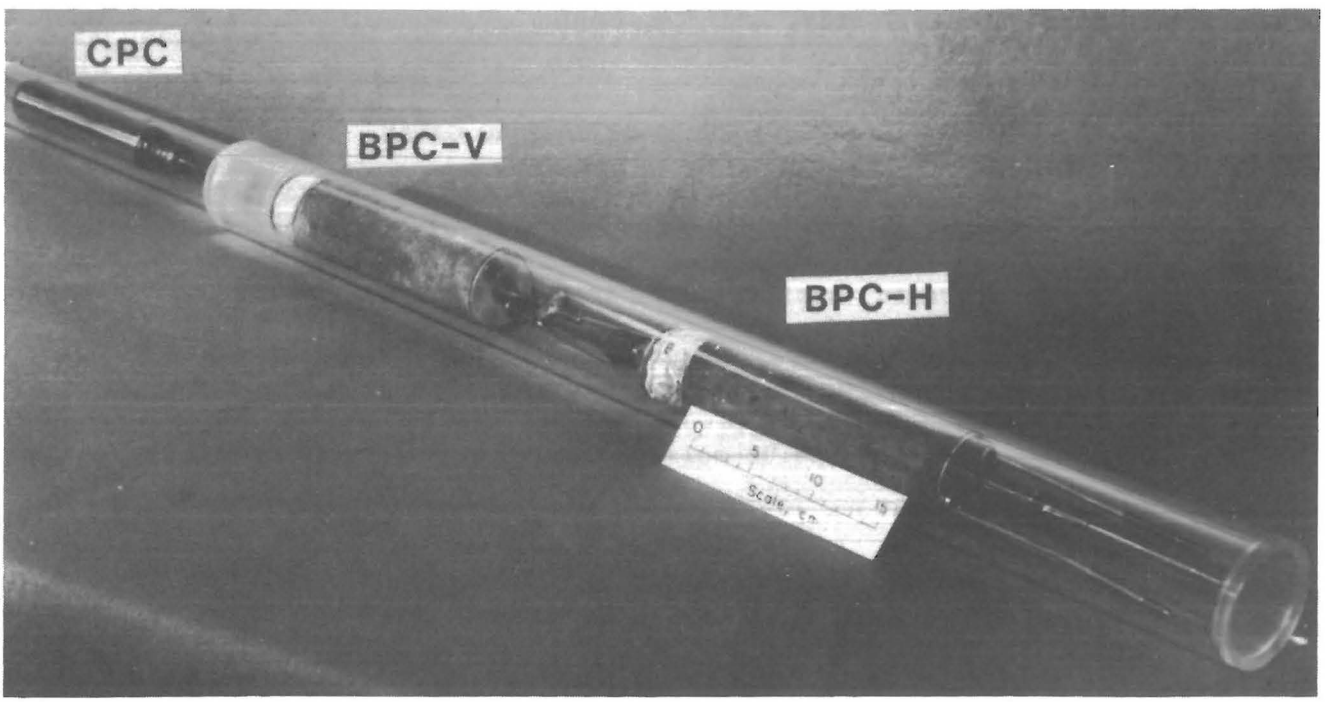

FIGURE B-1. - Hydraulic borehole pressure cell package consisting of one CPC and two BPC's.

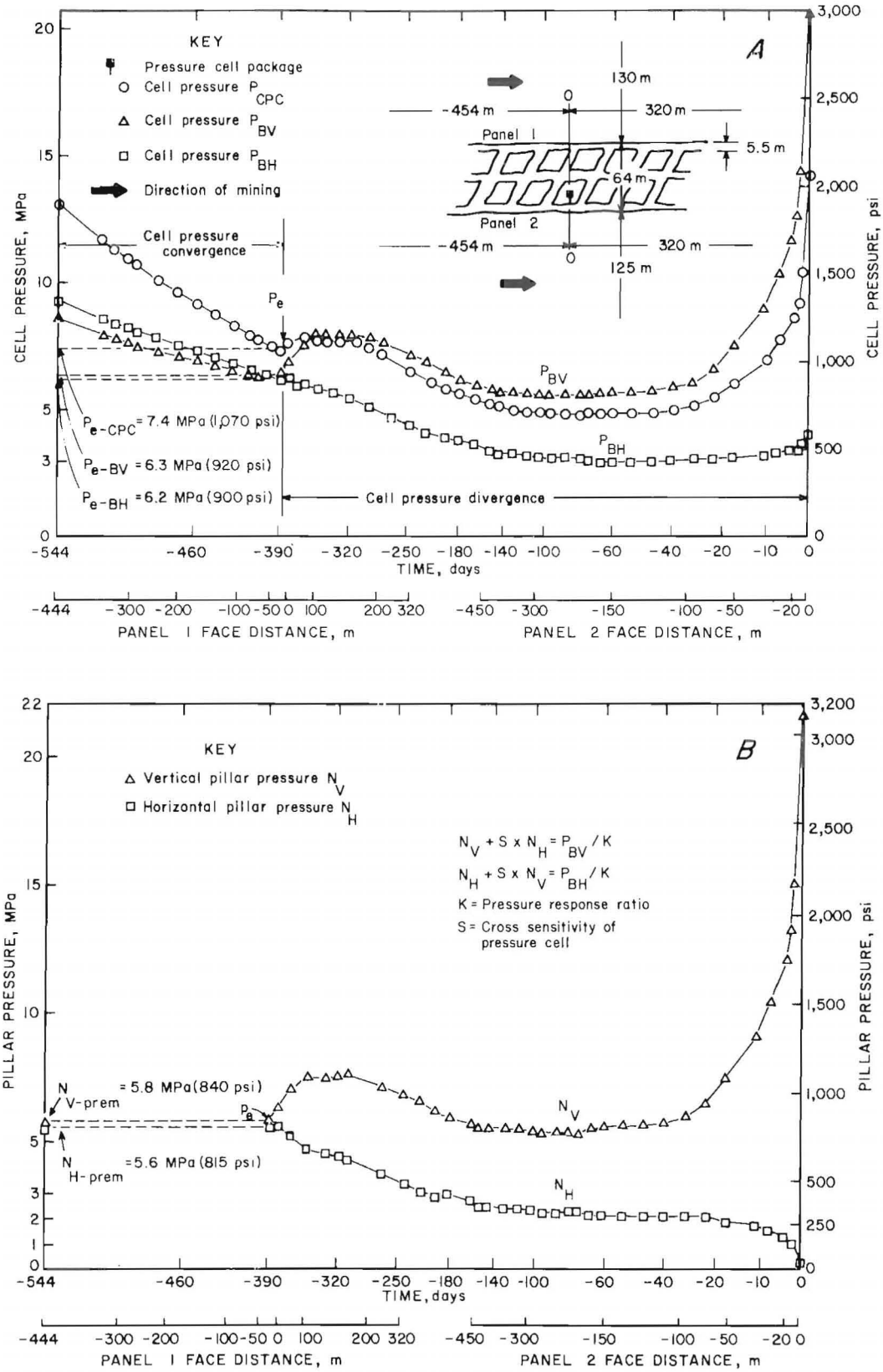

FIGURE B-2. - Mining-induced pillar loading. *A*, Cell pressures versus time and face distance to cells; *B*, vertical and horizontal pillar pressures versus time and face distance to cells.

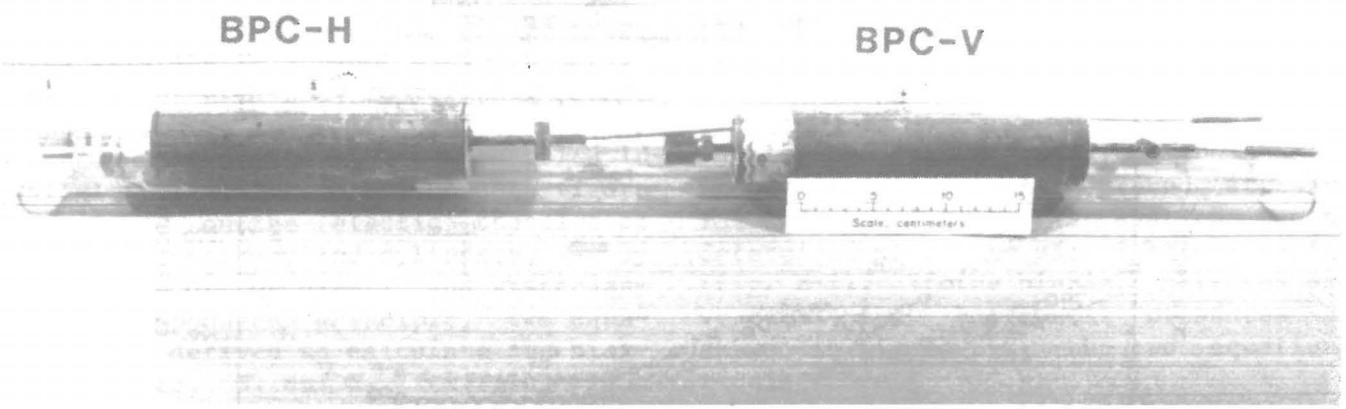

FIGURE B-3. - Hydraulic borehole pressure cell package consisting of two BPC's.

respectively, at the time of gauge reading. Thus with the cell pressure divergence curves of figure B-2*A*, the ground pressure histories shown in figure B-2*B* can be obtained.

The induced biaxial ground stresses (e.g., vertical and horizontal pressures) also can be measured and determined by a combination of only two BPC's installed in a single drill hole, as shown in figure B-3, if the pressure response ratio K, defined as the ratio of P_{BH} or P_{BV} to the effective directional ground pressure, is known. This response ratio K is determined by

$$K = P_{BH} / (N_H + S \times N_V)$$

or

$$K = P_{BV} / (N_V + S \times N_H), \qquad (B\text{-}5)$$

where N_H and N_V are derived from equations B-1 through B-4. Therefore, with known values of K and S, N_V and N_H can be calculated using equation B-5 and the P_{BV}, P_{BH} readings. The value of K varies with the rock type; for example, K_{coal} (tested with Pittsburgh seam) is 1.00±0.05 within 95-pct confidence interval from 24 tests.

☆U.S. GPO: 1985-505-019/20,026

INT.-BU.OF MINES,PGH.,PA. 27891